NASA TECHNICAL MEMORANDUM

NASA TM X-2951

NASA TM X-2951

THRUST PERFORMANCE OF ISOLATED PLUG NOZZLES WITH TWO TYPES OF 40-SPOKE NOISE SUPPRESSOR AT MACH NUMBERS FROM 0 TO 0.45

by Douglas E. Harrington and James J. Schloemer

Lewis Research Center

Cleveland, Ohio 44135

NATIONAL AERONAUTICS AND SPACE ADMINISTRATION • WASHINGTON, D. C. • JANUARY 1974

1. Report No.	2. Government Accession No.	3. Recipient's Catalog No.
NASA TM X-2951		

4. Title and Subtitle	5. Report Date
THRUST PERFORMANCE OF ISOLATED PLUG NOZZLES WITH TWO TYPES OF 40-SPOKE NOISE SUPPRESSOR AT MACH NUMBERS FROM 0 TO 0.45	January 1974
	6. Performing Organization Code

7. Author(s)	8. Performing Organization Report No.
Douglas E. Harrington, Lewis Research Center; and James J. Schloemer, General Electric Co., Cincinnati, Ohio.	E-7541
	10. Work Unit No. 501-24
9. Performing Organization Name and Address Lewis Research Center National Aeronautics and Space Administration Cleveland, Ohio 44135	11. Contract or Grant No.
	13. Type of Report and Period Covered Technical Memorandum
12. Sponsoring Agency Name and Address National Aeronautics and Space Administration Washington, D.C. 20546	14. Sponsoring Agency Code

15. Supplementary Notes

16. Abstract

Plug nozzles with two types of 40-spoke noise suppressor were tested at free-stream Mach numbers from 0 to 0.45 and over a range of nozzle pressure ratios from 1.5 to 4.0. In addition, an unsuppressed plug nozzle and a Supersonic Tunnel Association (STA) nozzle were also tested to provide baseline levels of thrust performance. The unsuppressed plug nozzle had an efficiency of 98 percent at an assumed takeoff pressure ratio of 3.0 and at Mach 0.36. At the same condition the suppressor nozzles had efficiencies of approximately 83.5 percent.

17. Key Words (Suggested by Author(s))		18. Distribution Statement
Exhaust Nozzles	Noise Suppression	Unclassified - unlimited
Nozzles	Jet Noise	
Plug Nozzles	Suppressor Nozzles	
		Cat. 28

19. Security Classif. (of this report)	20. Security Classif. (of this page)	21. No. of Pages	22. Price*
Unclassified	Unclassified	36	$3.00

* For sale by the National Technical Information Service, Springfield, Virginia 22151

Page Intentionally Left Blank

THRUST PERFORMANCE OF ISOLATED PLUG NOZZLES WITH TWO TYPES OF 40-SPOKE NOISE SUPPRESSOR AT MACH NUMBERS FROM 0 TO 0.45

by Douglas E. Harrington and James J. Schloemer*

Lewis Research Center

SUMMARY

Two 40-spoke noise suppressors were tested with plug nozzles in the Lewis 8- by 6-Foot Supersonic Wind Tunnel to determine thrust performance at takeoff conditions. These nozzles were designed primarily for application to advanced supersonic cruise aircraft in which a dry turbojet or mixed-flow turbofan engine would be used. An unsuppressed plug nozzle and a Supersonic Tunnel Association (STA) nozzle were also tested to determine baseline levels of thrust performance. The majority of the data were obtained at free-stream Mach numbers of 0 to 0.45 and nozzle pressure ratios of 1.5 to 4.0. However, the unsuppressed plug and the STA nozzles were also tested at Mach numbers of 0.8 and 0.9. Dry air at room temperature was supplied to the nozzles in the test.

The unsuppressed plug nozzle had a baseline nozzle efficiency of 98 percent at an assumed takeoff pressure ratio of 3.0 and at Mach 0.36. Both 40-spoke suppressor nozzles exhibited nozzle efficiencies of approximately 83.5 percent at this condition. This represents a decrement in nozzle efficiency of 14.5 percent when compared with the unsuppressed plug nozzle. Approximately 85 percent of this thrust loss (12.5 percent of ideal thrust) was attributed to spoke-base pressure drag. At a nozzle pressure ratio of 3.0, external flow had no appreciable effect on nozzle efficiencies up to Mach 0.45 for the square-spoke suppressor nozzle. This was reflected in the spoke-base pressure drag, where no external flow effects occurred. The vee-spoke suppressor nozzle, however, experienced a thrust loss of 1 to 2 percent due to external flow at Mach numbers from 0.36 to 0.45. This loss was again reflected in the spoke-base pressure drag, which increased with the addition of external flow.

*General Electric Co., Cincinnati, Ohio.

INTRODUCTION

Nozzle concepts appropriate for advanced supersonic cruise aircraft must operate efficiently over a wide range of flight conditions and engine power settings. The low-angle conical plug is a nozzle concept that offers the potential of good aerodynamic performance with a minimum of mechanical complexity. As a consequence, a number of tests have been conducted (refs. 1 to 11) to optimize the thrust performance, to investigate installation effects, and to determine the heat-transfer characteristics for this type of plug nozzle. In recent years, increasing emphasis has been placed on the reduction of aircraft noise. During takeoff and climb out, when the aircraft engines are at a high power setting, the dominant noise source is usually associated with the high velocity jet emanating from the exhaust nozzle. Jet noise characteristics for several nozzle types including a low-angle plug were evaluated at takeoff pressure ratios in a static test stand (ref. 12). However, takeoff and climb out speeds associated with advanced supersonic aircraft are relatively high (approximately Mach 0.35). Thus, the effect of external flow on jet noise must also be evaluated. Tests to evaluate flight velocity effects have been conducted and are reported in reference 13. A number of techniques to suppress jet noise are currently under investigation. One concept of interest, particularly for plug nozzles, is the multispoke suppressor. After takeoff the suppressor would be retracted and stowed either in the outer shroud or plug. To evaluate a suppressor concept like the multispoke, it is necessary to study a tradeoff between high noise suppression and good thrust performance (refs. 14 to 16).

This report presents the thrust performance for two 40-spoke suppressor plug nozzles tested in the Lewis 8- by 6-Foot Supersonic Wind Tunnel. These nozzles were designed primarily for application to advanced supersonic cruise aircraft in which a dry turbojet or mixed-flow turbofan engine would be used. An unsuppressed plug nozzle and a Supersonic Tunnel Association (STA) nozzle were also tested to determine baseline levels of thrust performance. The majority of the data were obtained at free-stream Mach numbers from 0 to 0.45 and nozzle pressure ratios from 1.5 to 4.0. However, the unsuppressed plug and the STA nozzles were also tested at Mach 0.8 and 0.9. Dry air at room temperature was supplied to the nozzles in this test. Angle of attack of the model was maintained at 0°. The range of Reynolds number was from 1.5×10^7 to 2.7×10^7.

APPARATUS AND PROCEDURE

Installation

The test nozzles were strut mounted in the test section of the wind tunnel as shown in figures 1 and 2. The support system consisted of a forward swept strut (30° sweep

angle) having a thickness to chord ratio of 0.07, and an ogive forebody with a maximum diameter of 15.24 centimeters (6.0 in.). Because the nozzles in this test were 20.32 centimeters (8 in.) in diameter, a transition section was necessary to adapt the support forebody diameter of 15.24 centimeters (6 in.) to the 20.32 (8.0 in.) nozzle diameter. This transition was 1.85 nozzle diameters long and consisted of two circular arcs tangent at the midpoint of this section. A cylindrical section approximately 3.5 nozzle diameters long was provided downstream of the transition. The cone-cylinder pressure data of reference 17 indicated that this length should have been sufficient upstream of the test nozzles to re-establish ambient flow conditions. The thrust-minus-drag of the exhaust nozzles was determined from the force- and flow-measuring section located just downstream of the transition section (fig. 2). The internal geometry of the model showing the details of the force- and flow-measuring section is shown in figure 3. Nozzle weight flow was determined using a choked convergent-divergent nozzle. Because the metering nozzle was choked, it was necessary to measure only total pressure and temperature. Total pressure upstream of the ASME nozzle P_1 was measured using a four-tube, area-weighted rake. Total temperature T_1 was measured by two shielded thermocouples. To determine the actual weight flow of the test nozzle, it was necessary to calculate a meter discharge coefficient. In addition, real gas effects were accounted for in the determination of weight flow (ref. 18).

The metric part of the model was cantilevered directly from the diverging section of the ASME flow metering nozzle. Two strain gage links were used to measure the force between the metric and grounded part of the model. A flexible seal at the throat of the ASME nozzle was used to separate the metric and grounded sections. The actual thrust-minus-drag of a test nozzle was then determined from the momentum entering the ASME metering nozzle, a balance force obtained from the two strain gage links, and various pressure-area terms. When testing with external flow, the thrust-minus-drag of the test nozzle as calculated above was modified to exclude the friction drag on the cylindrical surface from the metric break to the beginning of the test nozzles (approximately 1.3 model diameters). The friction drag on the cylindrical surface was estimated using the method of reference 19.

The nozzle airflow passes through a series of choke plates and screens to provide uniform flow at station 7. The nozzle total pressure at station 7 P_7 was determined by using two four-tube, area-weighted rakes. Nozzle total temperature T_7 was calculated by subtracting the temperature drop due to Joule-Thomson throttling of a real gas between stations 1 and 7. This temperature drop was calculated using a curve fit of tabulated properties of air from reference 20. The model pressures, except the high total pressure P_1, were determined from a scanner valve system. The procedure during a test run was to set a free-stream Mach number and then go through a variation in nozzle pressure ratio. Since for a given free-stream Mach number, tunnel static pressure was a constant, variations in nozzle pressure ratio were obtained by changing nozzle total

pressure, P_7.

Nozzle Geometry

The geometric details of the various nozzles tested are shown in figures 4 to 7. Pertinent area ratios are listed in table I.

The STA nozzle is shown in figure 4. This nozzle is basically a modified ASME nozzle with a circular-arc boattail. The STA nozzle was tested to provide a reference level of performance for this particular installation in the wind tunnel. The chordal boattail angle was 10.8°.

The unsuppressed plug nozzle is shown in figure 5. This nozzle provided a baseline level of performance for use in comparing with the performance of the suppressor nozzles that were evaluated in this test. The design pressure ratio of this nozzle, based on its internal expansion area ratio, was 3.4. The shroud had a 3.5° conical boattail and the plug had a 15° half angle.

The square-spoke plug nozzle geometric details are shown in figure 6. During takeoff and climb-out with this nozzle, spokes are deployed for jet noise suppression. After climb-out from the airport, the spokes are then retracted into the outer shroud for cruise. The nozzle will then take on the general appearance of the unsuppressed plug and should have relatively high performance. The square-spoke plug nozzle evaluated in this test had 40 spokes. Each of these spokes was slanted 15° from vertical to improve the mixing of the nozzle jet with the external flow, and, thus, to reduce jet noise. The spokes had a rectangular cross section and were essentially parallel sided. The geometric area ratio $(AR)_{geo}$ of this suppressor nozzle was approximately 1.55. The geometric area ratio is defined as the ratio of the annular flow area with spokes retracted to the flow area with spokes deployed. As with the unsuppressed plug nozzle, this nozzle had a 15° half-angle plug (except at the collapsed section, where it was cylindrical).

The vee-spoke plug nozzle geometric details are shown in figure 7. As with the square-spoke plug nozzle, the spokes of this concept would be deployed only during takeoff and climb-out. The vee-spokes, however, are more difficult to stow because of their larger size. Thus, they probably would have to be stowed in the plug rather than in the shroud. The vee-spoke nozzle evaluated in this test had 40 spokes. Each of the spokes was open and formed a "vee" (view A-A, fig. 7). The "vee" is intended to improve ventilation in the spoke-base region and to improve mixing of the nozzle jet with external flow for the purpose of noise suppression. In addition, the upper portion of each spoke was slanted back 15° (again, to direct outer part of flow in outward direction for improved mixing) and the lower portion of the spoke was slanted forward 15° (to increase thrust performance by directing the flow along the plug surface). Each spoke was parallel-

sided. The geometric area ratio $(AR)_{geo}$ was approximately 1.95.

The last configuration tested was a cylindrical shroud with a total pressure rake. It was used to determine the boundary-layer characteristics of the flow approaching the test nozzles. The rake was located at 45^{o} from top centerline of the model ($\varphi = 45^{o}$) and consisted of 10 tubes. Rake details are given in the next section.

Instrumentation

Instrumentation for all configurations tested is presented in figures 8 to 13. The static-pressure orifices are denoted by the solid symbols but do not necessarily represent the true circumferential location of the orifices. The accompanying tables give the correct circumferential location of each orifice and its axial location. For the STA nozzle the axial reference point ($X_{\beta} = 0$) is the tangent point of the nozzle boattail with the cylindrical section of the model. For the plug nozzles the axial reference point ($X = 0$) was chosen to be the location of the nozzle throat at the plug surface. Locations of the base pressures of the spokes of the suppressor nozzles are tabulated as a function of circumferential location and a dimensionless radius parameter R.

Component forces on the spokes and nozzle boattails were determined by a pressure-area integration and do not include friction drag. The details of the cylindrical shroud with the boundary-layer rake are shown in figure 12. As stated previously the rake was located at $\varphi = 45^{o}$ and comprised 10 tubes. The installation of the flow-angularity probe is shown in figure 13. This probe was used in conjunction with the suppressor nozzles in an attempt to determine the angle of the jet just downstream of the spokes. The probe was located at several radial locations. The probe was used only during quiescent running, and the calibration from reference 21 was used to determine local flow angularity.

RESULTS AND DISCUSSION

Nozzle efficiencies of the STA nozzle are presented in figure 14. At quiescent conditions a comparison was made between data measured during this test and data reported in reference 22. Data agreement was quite good and was well within one-half percent. Boattail pressure drag of the STA nozzle as measured over a range of Mach numbers and pressure ratios is shown in figure 15. The drag is presented in two ways, as a fraction of nozzle ideal thrust and as drag coefficients using model cross-sectional area as a reference. Over the range of Mach numbers and pressure ratios tested, boattail pressure drag was always less than 4 percent of the nozzle ideal thrust.

Nozzle efficiencies of the unsuppressed plug and the two 40-spoke, suppressor plug nozzles are presented as a function of nozzle pressure ratio in figure 16. Testing of the suppressor nozzles was conducted up to a Mach number of 0.45 only. However, the nozzle efficiencies of the unsuppressed plug at Mach 0.80 and 0.90 are also presented. For static conditions the two 40-spoke suppressors had the same nozzle efficiency at pressure ratios equal to or greater than three. The unsuppressed plug nozzle had a baseline nozzle efficiency of 98 percent at an assumed takeoff pressure ratio of 3.0 and at Mach 0.36. Both 40-spoke suppressor nozzles exhibited nozzle efficiencies of approximately 83.5 percent at the same condition. This represents a decrease in nozzle efficiency of 14.5 percent when compared with the unsuppressed plug nozzle.

The boattail pressure drag for the unsuppressed plug nozzle and the spoke-base drag for the suppressor nozzles are presented in figure 17. All drag components are presented as a fraction of nozzle ideal thrust. At all test Mach numbers the ratio of boattail pressure drag to nozzle ideal thrust for the unsuppressed plug decreased with increasing nozzle pressure ratio. The spoke-base pressure drag of the suppressor nozzles was high. At an assumed takeoff Mach number of 0.36 and pressure ratio of 3.0, the spoke-base pressure drag for both suppressor nozzles was about 12.5 percent of nozzle ideal thrust. This loss represents about 85 percent of the efficiency decrease incurred when compared with the unsuppressed plug nozzle (14.5 percent thrust loss, see fig. 16).

External flow had no effect on spoke-base pressure drag for the square-spoke suppressor nozzle (see figure 17). This would be expected due to the shielding of the base region of the spokes from the external flow by the outer shroud. No such shielding was afforded the base region of the vee-spokes, however. As a consequence, the vee-spoke base-pressure drag increased with the addition of external flow (see fig. 17).

Figure 18 presents the effect of external flow on nozzle efficiency at a pressure ratio of 3.0. External flow up to Mach 0.45 had no appreciable effect on nozzle efficiencies of the square-spoke suppressor nozzle. The vee-spoke suppressor nozzle, however, experienced a thrust loss of 1 to 2 percent because of external flow at Mach numbers from 0.36 to 0.45. These results are a reflection of the trends discussed earlier in figure 17.

Nozzle discharge coefficients of the unsuppressed plug and the 40-spoke suppressor plug nozzles are presented in figure 19. Nozzle discharge coefficients increased somewhat with increasing nozzle pressure ratio. Generally speaking, discharge coefficients should be insensitive to changes in nozzle pressure ratio once the nozzle is choked. The trend of increasing discharge coefficients may be associated with some swirl in the model upstream of the flow metering nozzle. If swirl was present, the instrumentation used with the flow metering nozzle may have been inadequate. However, these limitations would only slightly affect nozzle performance because of the thrust measuring system design. At a nozzle pressure ratio of 3.0 a 1-percent error in weight flow would result in only about a 0.3-percent error in nozzle efficiency.

Flow angularity just downstream of the spokes for the two suppressor nozzles was determined and is shown in figure 20. This part of the test was conducted at quiescent conditions only and over a range of pressure ratios from 2.5 to 3.5 for three radial locations. Flow angle α is the angle of the flow relative to the nozzle centerline. The arrows represent flow angle only and are not intended to give an indication of the local Mach number. As can be seen in figure 20(a) the 15° aft slanted square spokes had the effect of directing the flow outward at higher pressure ratios. However, this did not occur with the vee-spoke suppressor, as the flow was generally directed down the plug (fig. 20(b)).

Boundary-layer velocity profiles of the model at an axial station approximately nine model diameters downstream of the nose are presented in figure 21. Also included are the normalized boundary-layer displacement thickness δ^*/d_m and momentum thickness δ^{**}/d_m. Estimates for sizing the boundary-layer rake were incorrect because the boundary-layer thickness turned out to be thicker than estimated. Attempts were made to determine the approximate boundary-layer thickness by extrapolating the velocity profiles. Displacement and momentum thicknesses were determined by using the extrapolated velocity profile curves.

Internal and external static-pressure distributions are presented in figures 22 to 27. Distributions are shown at pertinent Mach numbers and nozzle pressure ratios. Of particular interest are the spoke-base pressure distributions, which are shown in figures 25 and 27.

SUMMARY OF RESULTS

Two 40-spoke suppressor plug nozzles were tested in the Lewis 8- by 6-Foot Supersonic Wind Tunnel to determine thrust performance at takeoff conditions. These nozzles were designed primarily for application to advanced supersonic cruise aircraft in which a dry turbojet or mixed-flow turbofan engine would be used. After takeoff the suppressor would be retracted and stowed either in the outer shroud or the plug. An unsuppressed plug nozzle and a Supersonic Tunnel Association (STA) nozzle were also tested to determine baseline levels of thrust performance. The majority of the data were obtained at free-stream Mach numbers of 0 to 0.45 and nozzle pressure ratios of 1.5 to 4.0. However, the unsuppressed plug and the STA nozzles were also tested at Mach 0.8 and 0.9. Dry air at room temperature was supplied to the nozzles in the test. The results of the test were as follows:

1. The unsuppressed plug nozzle had a baseline nozzle efficiency of 98 percent at an assumed takeoff pressure ratio of 3.0 and Mach number of 0.36.

2. Both 40-spoke suppressor nozzles exhibited nozzle efficiencies of approximately

83.5 percent at the assumed takeoff condition. This represents a 14.5 percent decrease in nozzle efficiency when compared with the unsuppressed plug nozzle.

3. Approximately 85 percent of the efficiency decrement experienced by the suppressor nozzles at the takeoff condition was due to spoke-base pressure drag. This loss represents about 12.5 percent of nozzle ideal thrust.

4. At a nozzle pressure ratio of 3.0, external flow up to Mach 0.45 had no appreciable effect on nozzle efficiencies of the square-spoke suppressor nozzle. This was reflected in the spoke-base pressure drag, where no external flow effect occurred because of the shielding of the base region by the outer shroud. The vee-spoke suppressor nozzle, however, experienced a thrust loss of approximately 1 to 2 percent because of external flow at Mach numbers from 0.36 to 0.45. This loss was again reflected in the spoke-base pressure drag, which increased with the addition of external flow.

Lewis Research Center,
National Aeronautics and Space Administration,
Cleveland, Ohio, August 16, 1973,
501-24.

APPENDIX - SYMBOLS

A	cross-sectional area
$(AR)_{eff}$	effective area ratio; ratio of the annular flow area with spokes retracted to the effective flow area with spokes deployed
$(AR)_{geo}$	geometric area ratio; ratio of the annular flow area with spokes retracted to the actual flow area with spokes deployed
C_D	nozzle discharge coefficient
$C_{D\beta}$	boattail pressure drag coefficient
C_p	pressure coefficient, $(p - p_o)/q_o$
D	pressure drag
D_t	total external drag (viscous and pressure)
d	diameter
F	nozzle gross thrust
$(F\text{-}D)_t/F_i$	nozzle efficiency (or gross thrust coefficient)
M	Mach number
P	total pressure
p	static pressure
q	dynamic pressure
r	radial distance from nozzle axis
r_{pl}	plug radius at nozzle geometric throat ($X = 0$)
r_{sh}	outer-shroud internal radius at nozzle geometric throat ($X = 0$)
R	radius parameter, $(r - r_{pl})/(r_{sh} - r_{pl})$
V	velocity
X	axial distance downstream of geometric nozzle throat on plug surface
X_β	axial distance downstream of boattail tangency point (Supersonic Tunnel Association nozzle only)
y	radial distance measured from model surface
α	flow angle relative to nozzle centerline

δ^*	boundary-layer displacement thickness
δ^{**}	boundary-layer momentum thickness
φ	circumferential angle measured from top of nacelle in a clockwise direction (looking upstream)

Subscripts:

i	ideal (based on actual weight flow)
m	maximum nozzle diameter
pl	plug
sp	spoke
β	boattail
0	free stream station
1	flow measuring station
7	nozzle inlet station
8	nozzle throat station

REFERENCES

1. Bresnahan, Donald L.; and Johns, Albert L.: Cold Flow Investigation of a Low Angle Turbojet Plug Nozzle with Fixed Throat and Translating Shroud at Mach Numbers from 0 to 2.0. NASA TM X-1619, 1968.

2. Wasko, Robert A.; and Harrington, Douglas E.: Performance of a Collapsible Plug Nozzle Having Either Two-Position Cylindrical or Variable Angle Floating Shrouds at Mach Numbers from 0 to 2.0. NASA TM X-1657, 1968.

3. Bresnahan, Donald L.: Experimental Investigation of a 10^{o} Conical Turbojet Plug Nozzle with Translating Primary and Secondary Shrouds at Mach Numbers from 0 to 2.0. NASA TM X-1777, 1969.

4. Johns, Albert L.: Quiescent-Air Performance of a Truncated Turbojet Plug Nozzle with Shroud and Plug Base Flows from a Common Source. NASA TM X-1807, 1969.

5. Harrington, Douglas E.: Performance of a 10^{o} Conical Plug Nozzle with Various Primary Flap and Nacelle Configurations at Mach Numbers from 0 to 1.97. NASA TM X-2086, 1970.

6. Harrington, Douglas E.: Performance of Convergent and Plug Nozzles at Mach Numbers from 0 to 1.97. NASA TM X-2112, 1970.

7. Huntley, Sidney C.; and Samanich, Nick E.: Performance of a 10^{o} Conical Plug Nozzle Using a Turbojet Gas Generator. NASA TM X-52570, 1969.

8. Samanich, Nick E.; and Chamberlin, Roger: Flight Investigation of Installation Effects on a Plug Nozzle Installed on an Underwing Nacelle. NASA TM X-2295, 1971.

9. Jeracki, Robert J.; and Chenoweth, Francis C.: Cooland Flow Effects on the Performance of a Conical Plug Nozzle at Mach Numbers from 0 to 2.0. NASA TM X-2076, 1970.

10. Chenoweth, Francis C.; and Lieberman, Arthur: Experimental Investigation of Heat-Transfer Characteristics of a Film-Cooled Plug Nozzle with Translating Shroud. NASA TN D-6160, 1971.

11. Clark, John S.; and Lieberman, Arthur: Thermal Design Study of an Air-Cooled Plug-Nozzle System for a Supersonic-Cruise Aircraft. NASA TM X-2475, 1972.

12. Darchuk, George V.; and Balombin, Joseph R.: Noise Evlauation of Four Exhaust Nozzles for Afterburning Turbojet Engine. NASA TM X-2014, 1970.

13. Burley, Richard R.; and Karabinus, Raymond J.: Flyover and Static Tests to Investigate External Flow Effect on Jet Noise For Non-Suppressor and Suppressor Exhaust Nozzles. NASA TM X-68161, 1972.

14. Bresnahan, Donald L.: Internal Performance of a 10^{o} Concial Plug Nozzle with a Multispoke Primary and Translating External Shroud. NASA TM X-2573, 1972.

15. Johns, Albert L.: Internal Performance of a Wedge Nozzle for a Supersonic-Cruise Aircraft with a Multispoke Primary for Noise Suppression. NASA TM X-2689, 1973.

16. Brausch, J. F.: Flight Velocity Influence on Jet Noise of Conical Ejector, Annular Plug and Segmented Suppressor Nozzles. General Electric Co. (NASA CR-120961), Aug. 1972.

17. Blaha, Bernard J.; and Bresnahan, Donald L.: Wind Tunnel Installation Effects on Isolated Afterbodies at Mach Numbers from 0.56 to 1.5. NASA TM X-52581, 1969.

18. Johnson, Robert C.: Real-Gas Effects in Critical-Flow-Through Nozzles and Tabulated Thermodynamic Properties. NASA TN D-2565, 1965.

19. Smith, K. D.: Methods and Charts for Estimating Skin Friction Drag in Wind Tunnel Tests with Zero Heat Transfer. Rep. ARC-CP-824, Aeronautical Research Council, Great Britain, 1965.

20. Hilsenrath, Joseph; et al.: Tables of Thermal Properties of Gases. Circ. 564, National Bureau of Standards, Nov. 1, 1955.

21. Blaha, Bernard J.: Wind Tunnel Investigation of the Flow Field Under a 60-Degree Swept Wing at Mach Numbers from 0.6 to 2.6. NASA TM X-52585, 1969.

22. Kuehner, W.D.; Oller, T.L.; Staid, P.S.; and Twiss, C.T.: High Mach Exhaust Nozzles Program. Rep. TM 72-951, General Electric Co., Jan. 1973.

TABLE I. - PERTINENT AREA RATIOS[a]

Nozzle	A_β/A_m	A_8/A_m	A_{sp}/A_m	A_{pl}/A_m	$(AR)_{geo}$	$(AR)_{eff}$	C_D (nominal)
Supersonic tunnel association	0.74	0.25	----	----	----	----	0.99
Unsuppressed plug	.15	.26	----	0.58	----	----	.99
Square-spoke suppressor nozzle	.15	.33	0.19	.33	1.55	1.78	.87
Vee-spoke suppressor nozzle	.16	.28	.28	.30	1.95	2.03	.96

[a]All areas are areas projected on a plane perpendicular to nozzle axis (except A_8, which is the actual geometric throat area).

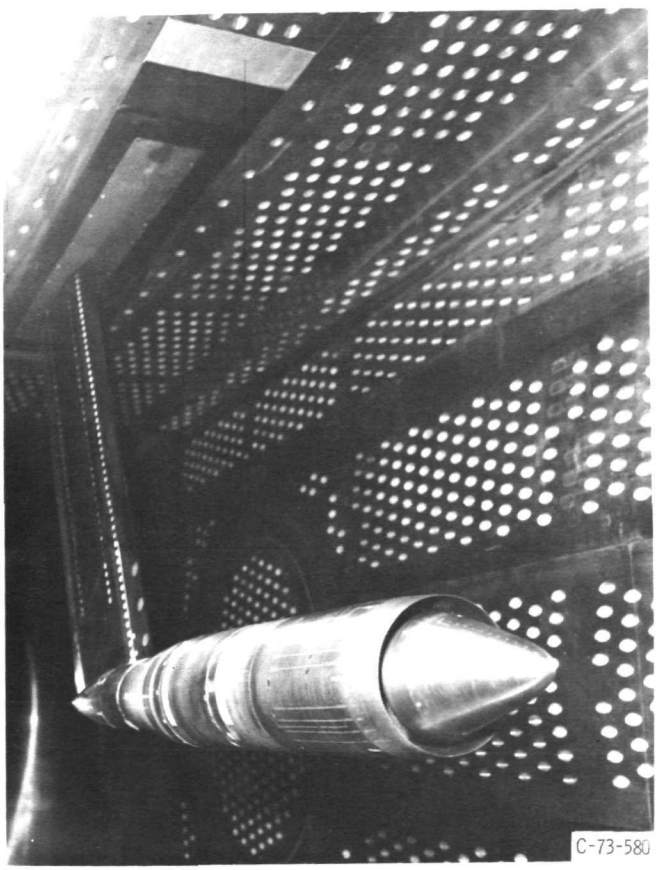

Figure 1. - Model installed in 8- by 6-Foot Supersonic Tunnel.

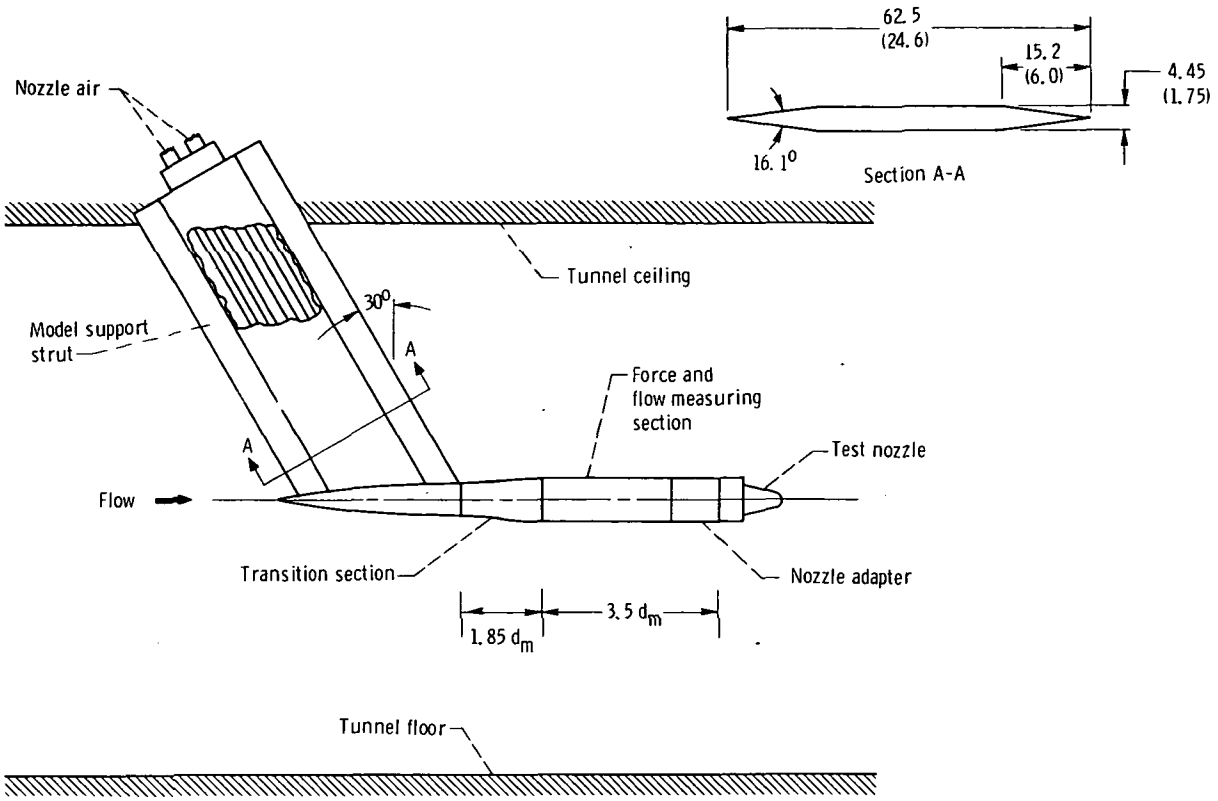

Figure 2. - Model installed in 8- by 6-Foot supersonic tunnel. (All dimensions are in cm (in.).

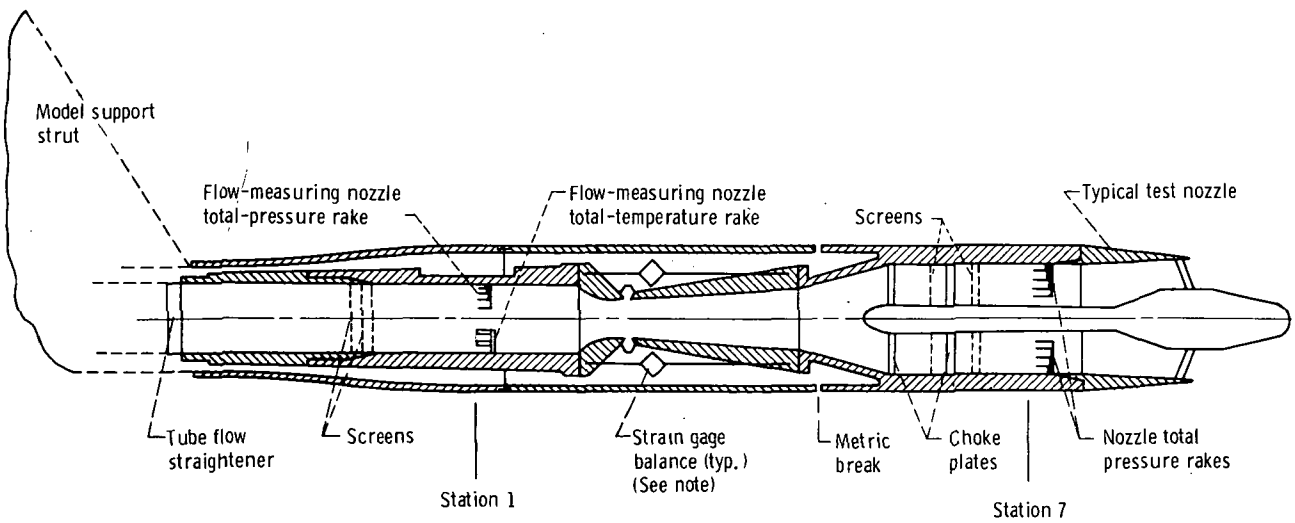

Figure 3. - Model internal geometry and thrust measuring system. Note: Strain gages actually located at $\varphi = 90^0$ and 270^0 ($\varphi = 0^0$ at top of model).

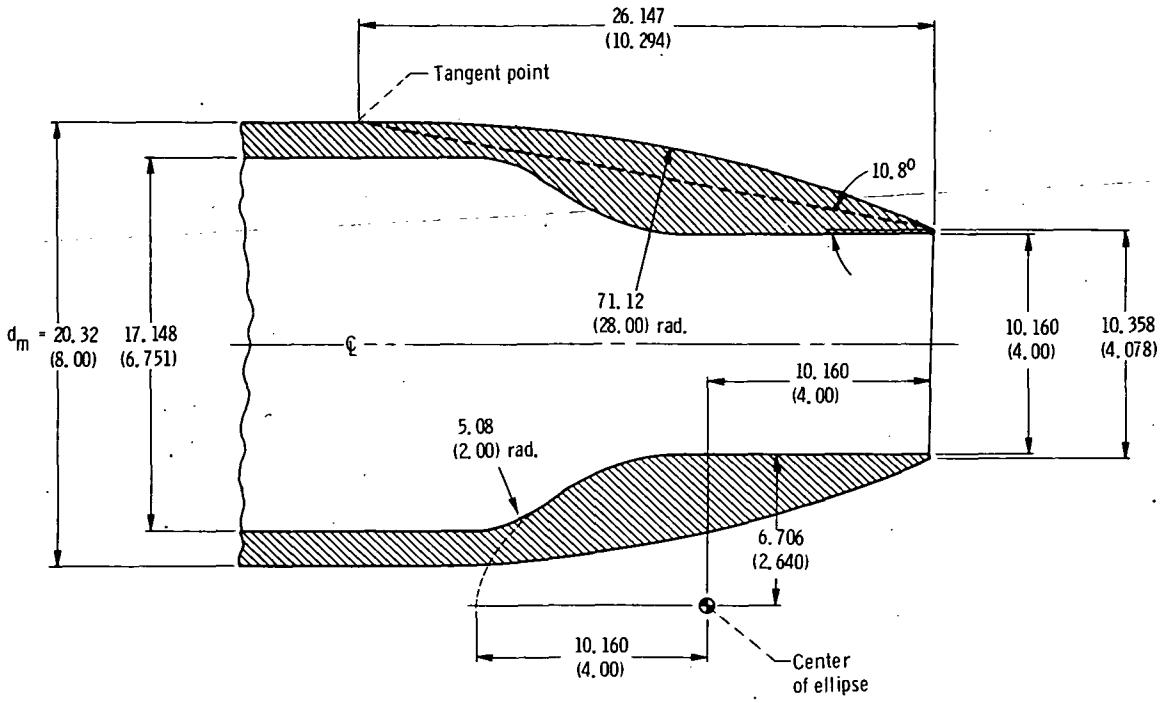

Figure 4. - Supersonic tunnel association (STA) nozzle geometric details. (All dimensions are in cm (in.).)

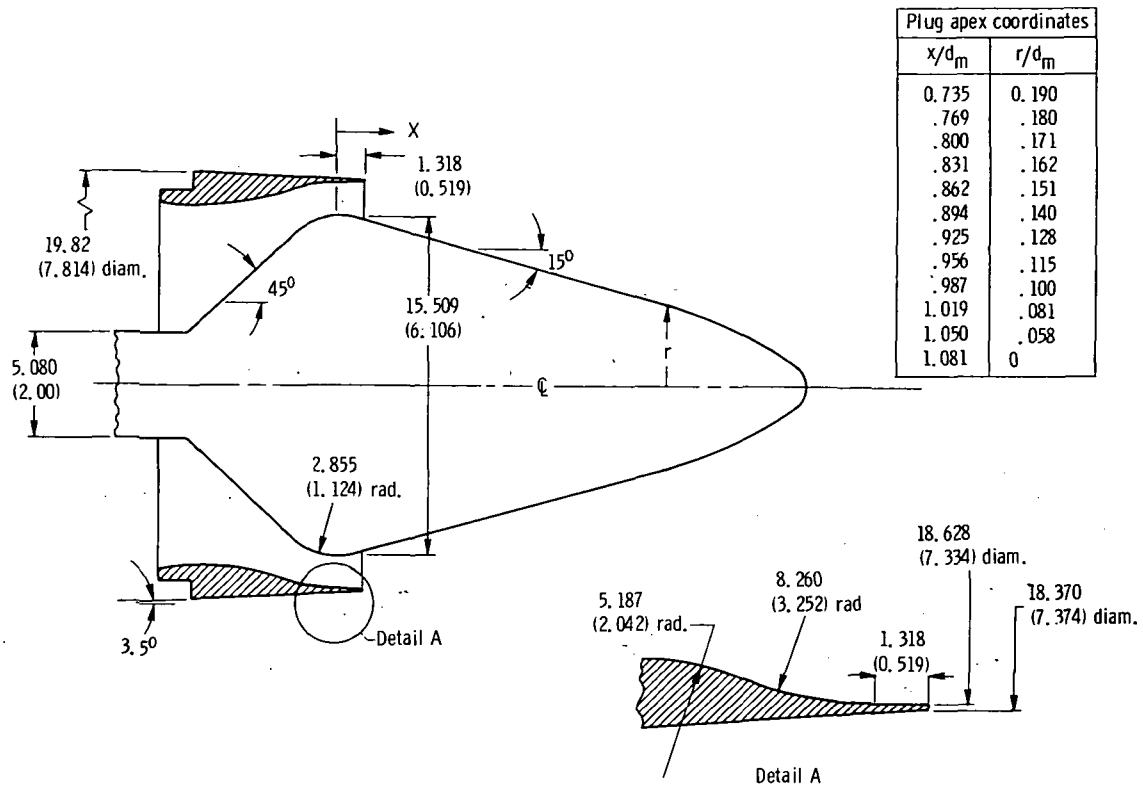

Plug apex coordinates	
x/d_m	r/d_m
0.735	0.190
.769	.180
.800	.171
.831	.162
.862	.151
.894	.140
.925	.128
.956	.115
.987	.100
1.019	.081
1.050	.058
1.081	0

Figure 5. - Unsuppressed plug nozzle geometric details. (All dimensions are in cm (in.).)

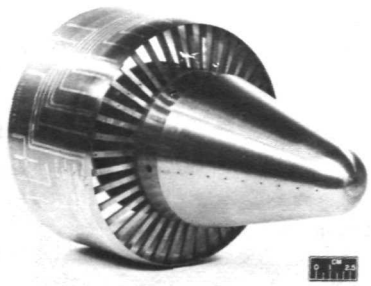

C-73-570

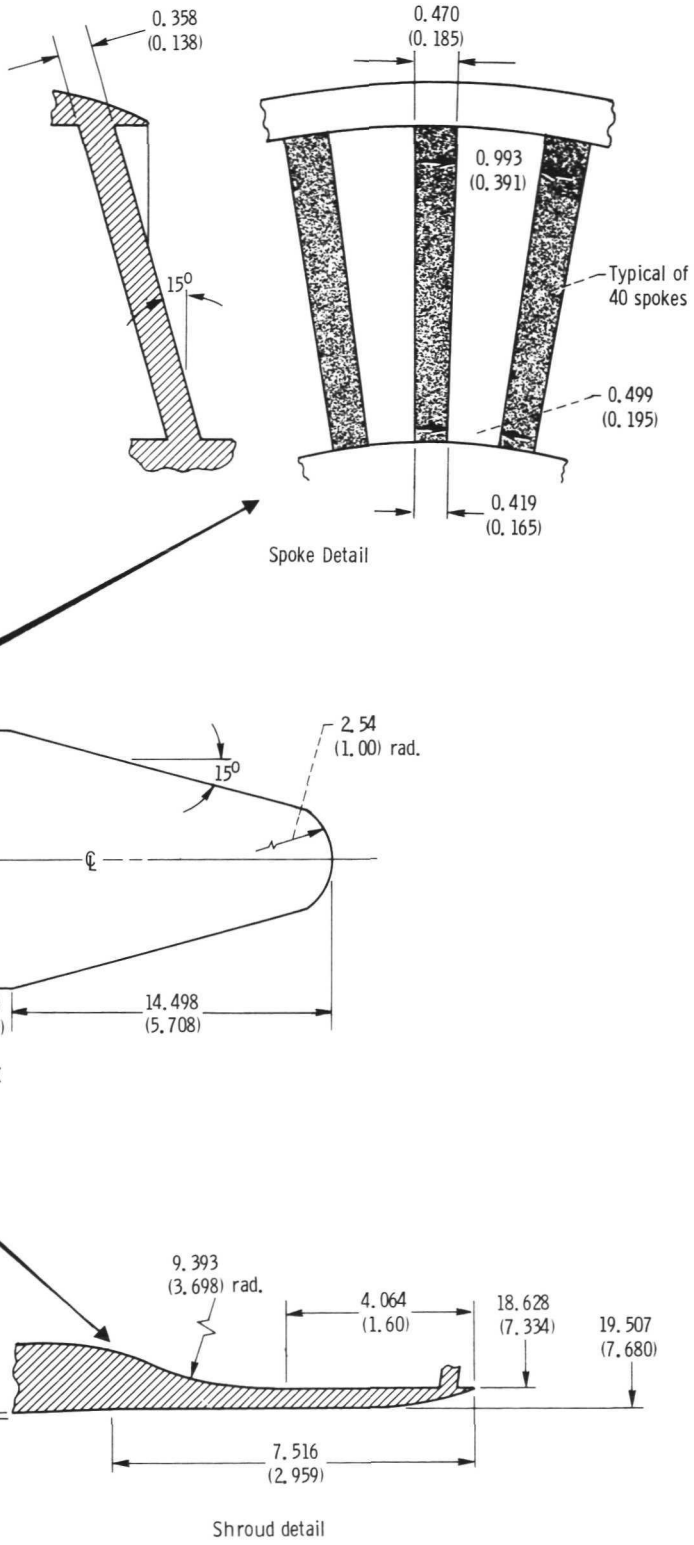

Figure 6. - Square-spoke plug nozzle geometric details. (All dimensions are in cm (in.))

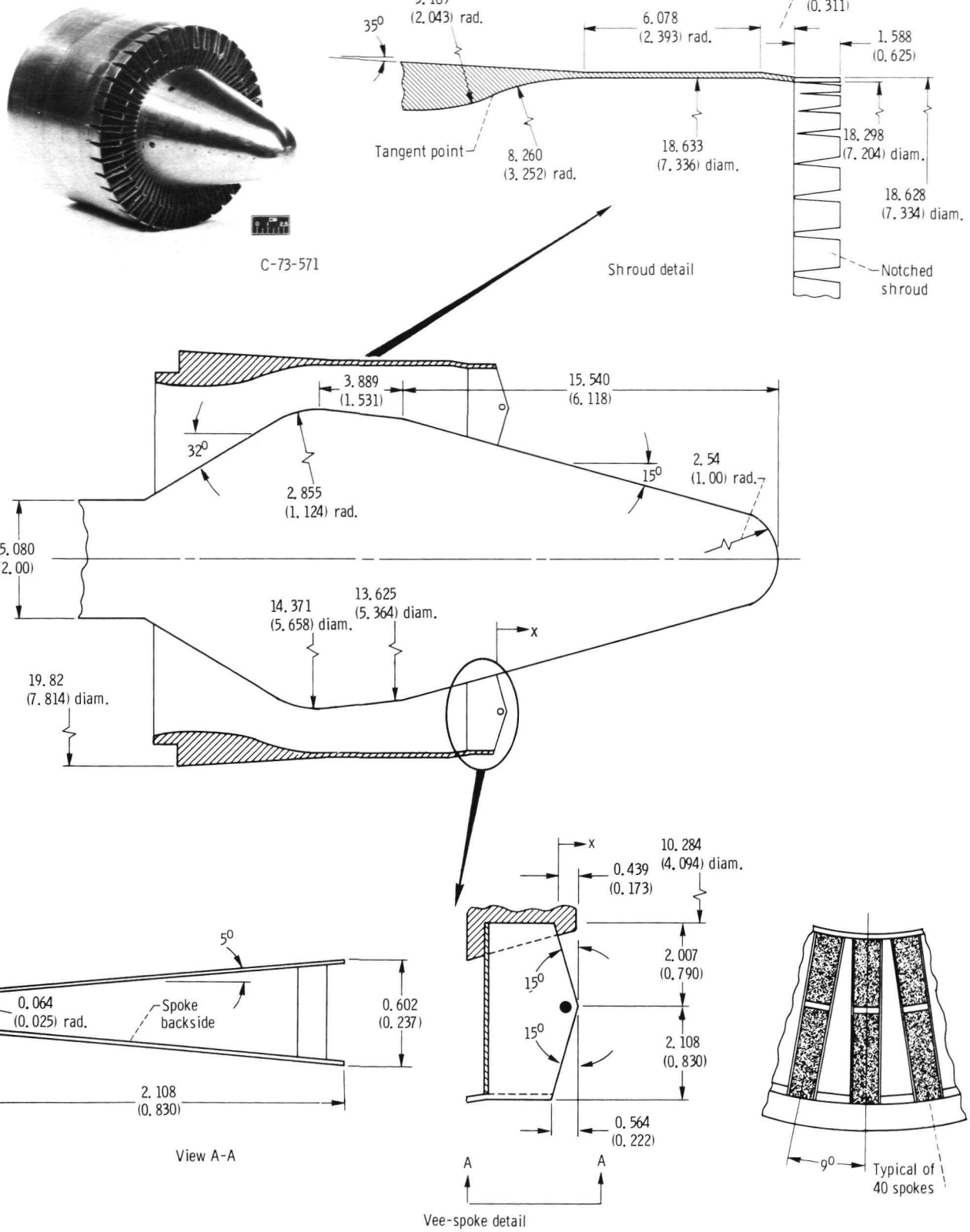

Figure 7. - Vee-spoke plug nozzle geometric details. (All dimensions are in cm (in.).)

Static pressure locations

Orifice number	Axial location, x_β/d_m	Circumferential location, φ, deg	Orifice number	Axial location, x_β/d_m	Circumferential location, φ, deg
1	-0.167	0	16	0.746	90
2	0		17	.927	
3	.193		18	1.107	
4	.373		19	1.197	
5	.566		20	1.274	
6	.746		21	-.167	180
7	.927		22	0	
8	1.107		23	.193	
9	1.197		24	.373	
10	1.274		25	.566	
11	-.167	90	26	.746	
12	0		27	.927	
13	.193		28	1.107	
14	.373		29	1.197	
15	.566		30	1.274	

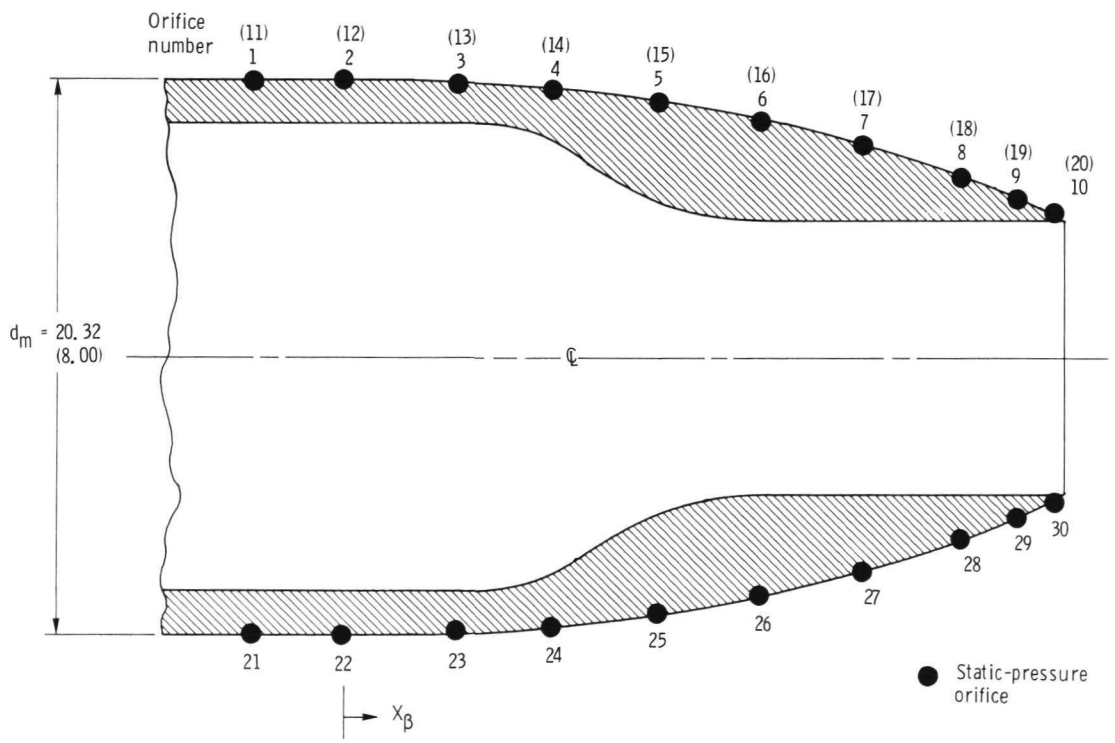

Figure 8. - Supersonic Tunnel Association (STA) boattail pressure instrumentation. Note: Orifice numbers in parenthesis denote orifices located at $\varphi = 90^0$ ($\varphi = 0^0$ at top of model).

Orifice number	Axial location, x/d_m	Circumferential location, φ, deg	Type of static pressure	Orifice number	Axial location, x/d_m	Circumferential location, φ, deg	Type of static pressure
1	-0.28	0	External	18	0	30	Plug
2	-.21	↓	↓	19	.04	↓	↓
3	-.14	↓	↓	20	.08	↓	↓
4	-.07	↓	↓	21	.16	↓	↓
5	0	↓	↓	22	.23	21	↓
6	.06	↓	↓	23	.30	↓	↓
7	-.16	↓	Internal	24	.37	↓	↓
8	-.13	↓	↓	25	.44	↓	↓
9	-.09	↓	↓	26	.51	↓	↓
10	-.06	↓	↓	27	.58	↓	↓
11	-.03	↓	↓	28	.65	↓	↓
12	0	↓	↓	29	.72	↓	↓
13	.03	↓	↓	30	.80	↓	↓
14	.05	↓	↓	31	.87	↓	↓
15	-.11	30	Plug	32	.94	↓	↓
16	-.07	30	Plug	33	1.01	↓	↓
17	-.04	30	Plug	34	1.08	↓	↓

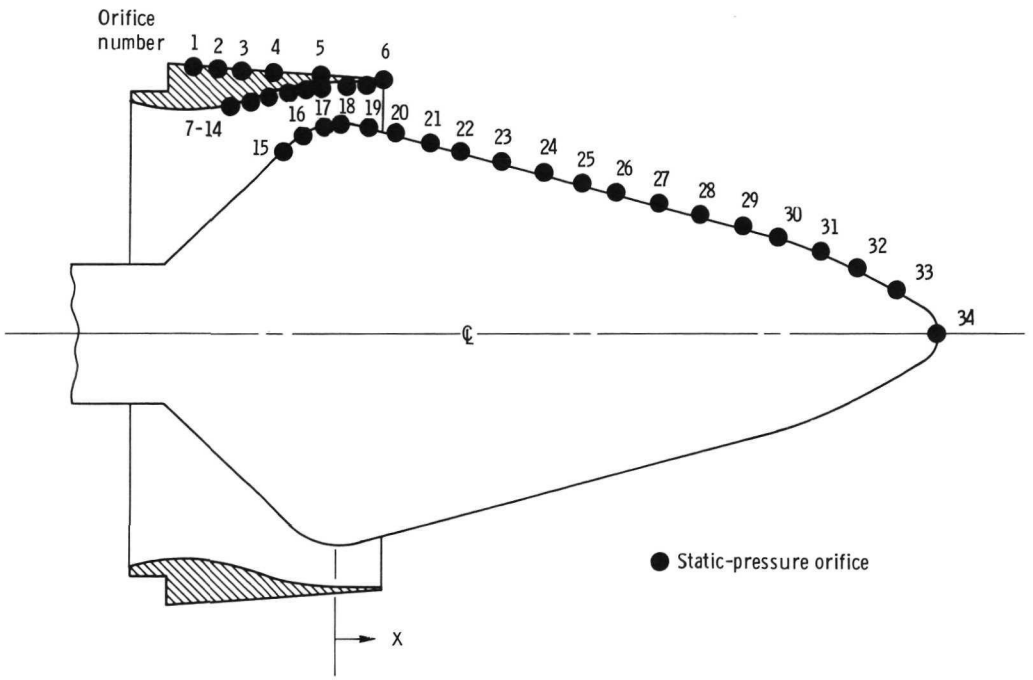

Figure 9. - Unsuppressed plug nozzle static-pressure instrumentation.

Orifice number	Axial location, x/d_m	Circumferential location, φ, deg	Type of static pressure	Orifice number	Axial location, x/d_m	Circumferential location, φ, deg	Type of static pressure
1	-0.43	0	External	18	-0.03	13.5	Plug
2	-.22			19	.01	9	
3	-.16			20	.07	0	
4	-.11			21	.12		
5	-.05			22	.16		
6	-.36		Internal	23	.23		
7	-.29			24	.29		
8	-.23			25	.36		
9	-.18			26	.43		
10	-.14			27	.50		
11	-.10			28	.57		
12	-.07			29	.64		
13	-.30		Plug	30	.71		
14	-.25			31	.79		
15	-.20			32	.86		
16	-.16			--	----		
17	-.12			--	----		

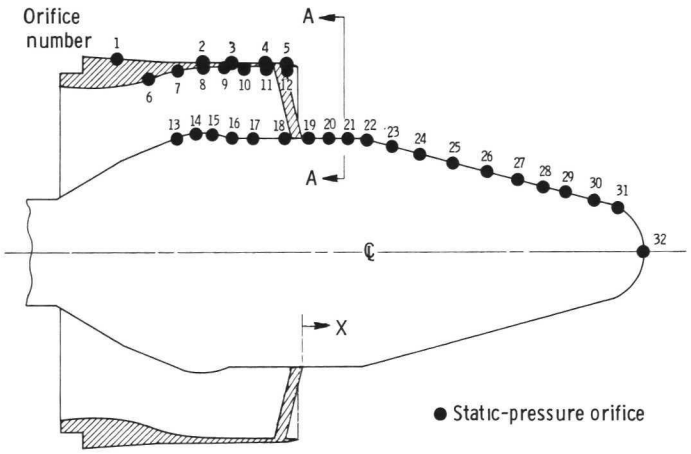

Square-spoke base static pressures		
Orifice number	Radial location. R	Circumferential location. φ, deg
1	0.91	0
2	.82	9
3	.74	18
4	.65	27
5	.65	27
6	.55	45
7	.47	54
8	.37	63
9	.27	72
10	.17	81
11	.06	90
12	.06	90

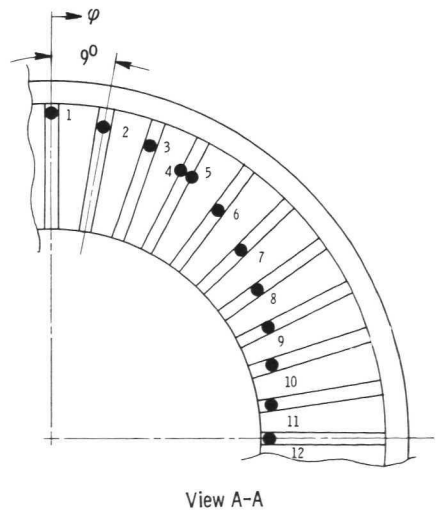

Figure 10. - Square-spoke plug nozzle static-pressure instrumentation.

Orifice number	Axial location, x/d_m	Circumferential location, φ, deg	Type of static pressure	Orifice number	Axial location, x/d_m	Circumferential location, φ, deg	Type of static pressure
1	-0.61	90	External	16	-0.34	0	Plug
2	-.42			17	-.30		
3	-.32			18	-.23		
4	-.12			19	-.19		
5	-.58	0	Internal	20	-.12		
6	-.53			21	.04		
7	-.47			22	.09		
8	-.42			23	.16		
9	-.34			24	.23		
10	-.24			25	.30		
11	-.13			26	.38		
12	-.50		Plug	27	.45		
13	-.46			28	.52		
14	-.42			29	.59		
15	-.38			30	.66		

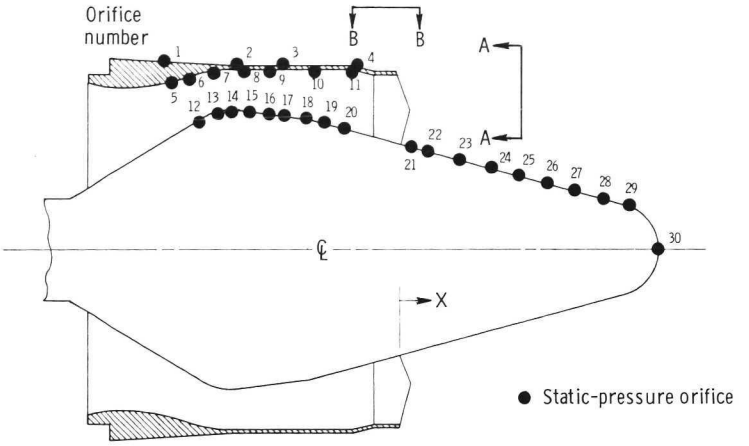

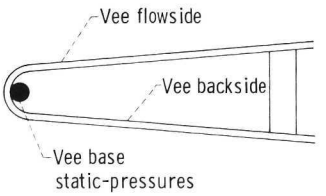

View B-B

Orifice number	Radial location, R	Circumferential location, φ, deg
1	0.86	0
2	.78	18
3	.69	27
4	.60	36
5	.52	63
6	.43	72
7	.34	81
8	.26	99
9	.17	108
10	.09	117

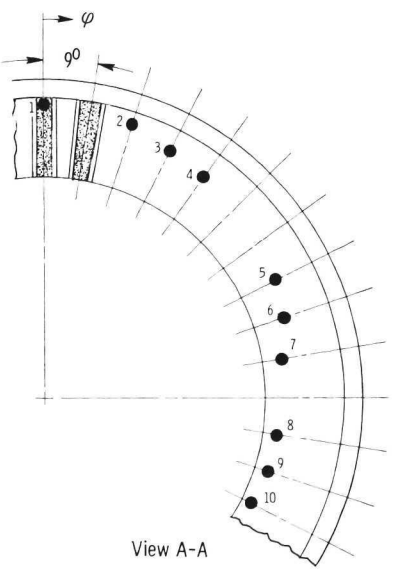

View A-A

Figure 11. - Vee-spoke plug nozzle static-pressure instrumentation.

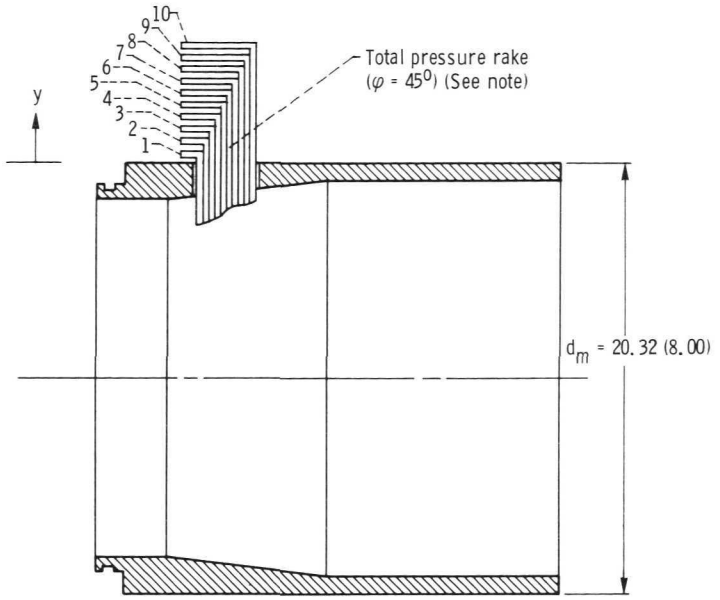

Tube number	Tube location, y/d_m
1	0.010
2	.020
3	.029
4	.039
5	.049
6	.058
7	.067
8	.077
9	.102
10	.126

Figure 12. - Boundary-layer shroud total-pressure tap locations. Note: Located at approximately nine nozzle diameters downstream of nose.

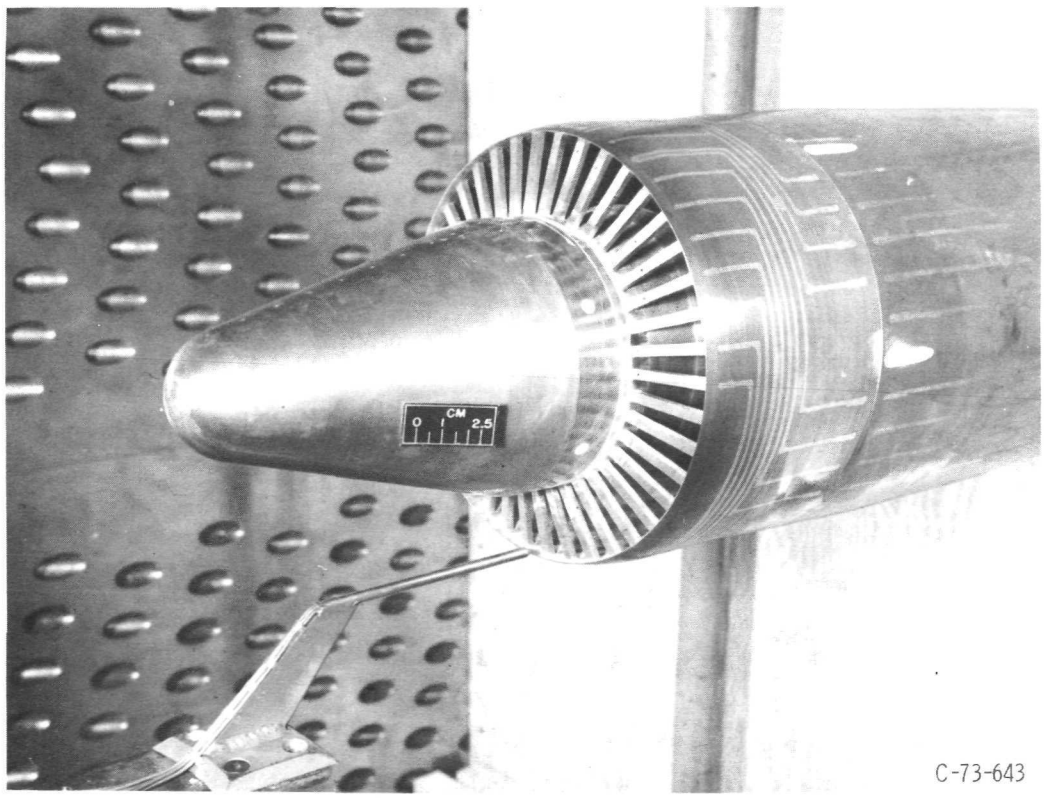

Figure 13. - Flow-angularity probe installation.

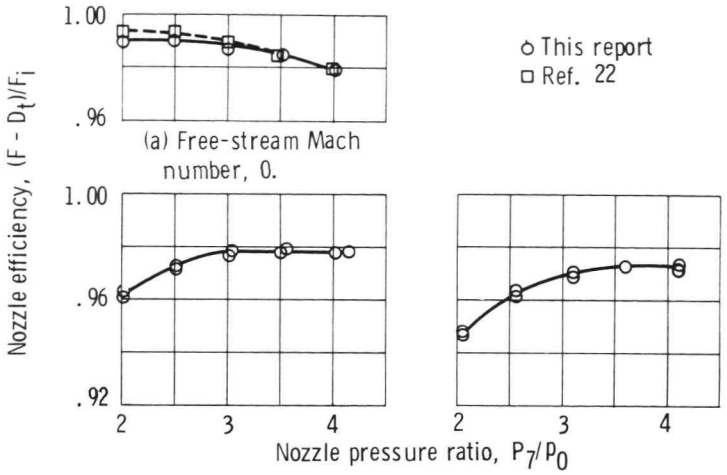

Figure 14. - Comparison of Supersonic Tunnel Association nozzle efficiencies from two facilities.

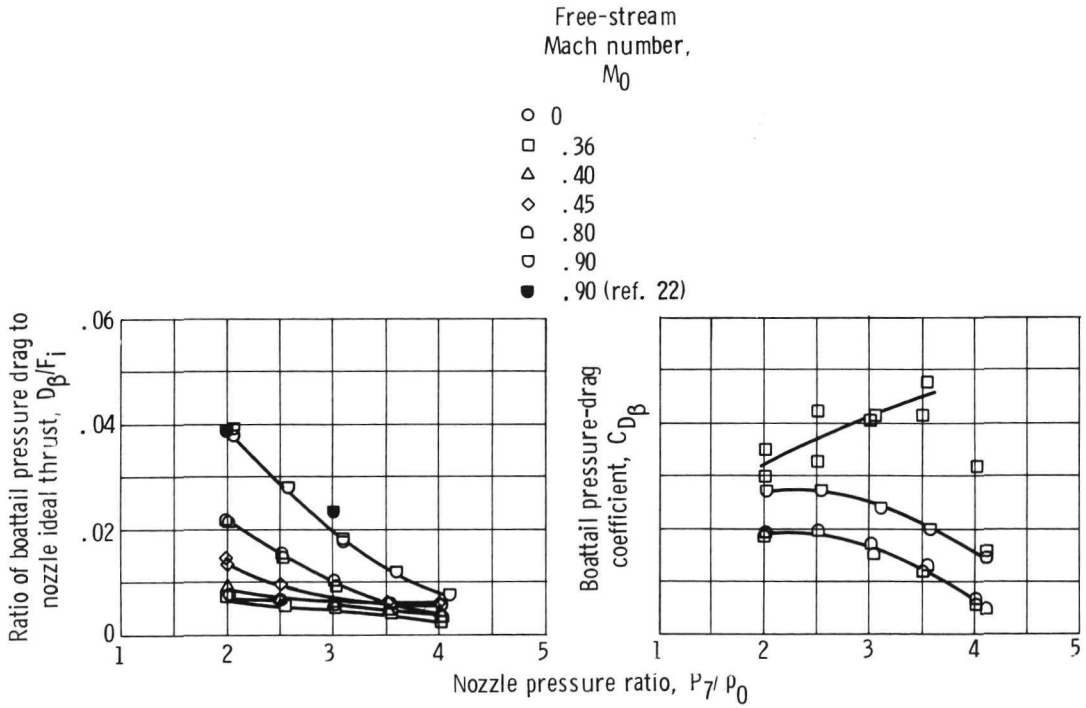

Figure 15. - Supersonic Tunnel Association (STA) nozzle boattail pressure drag.

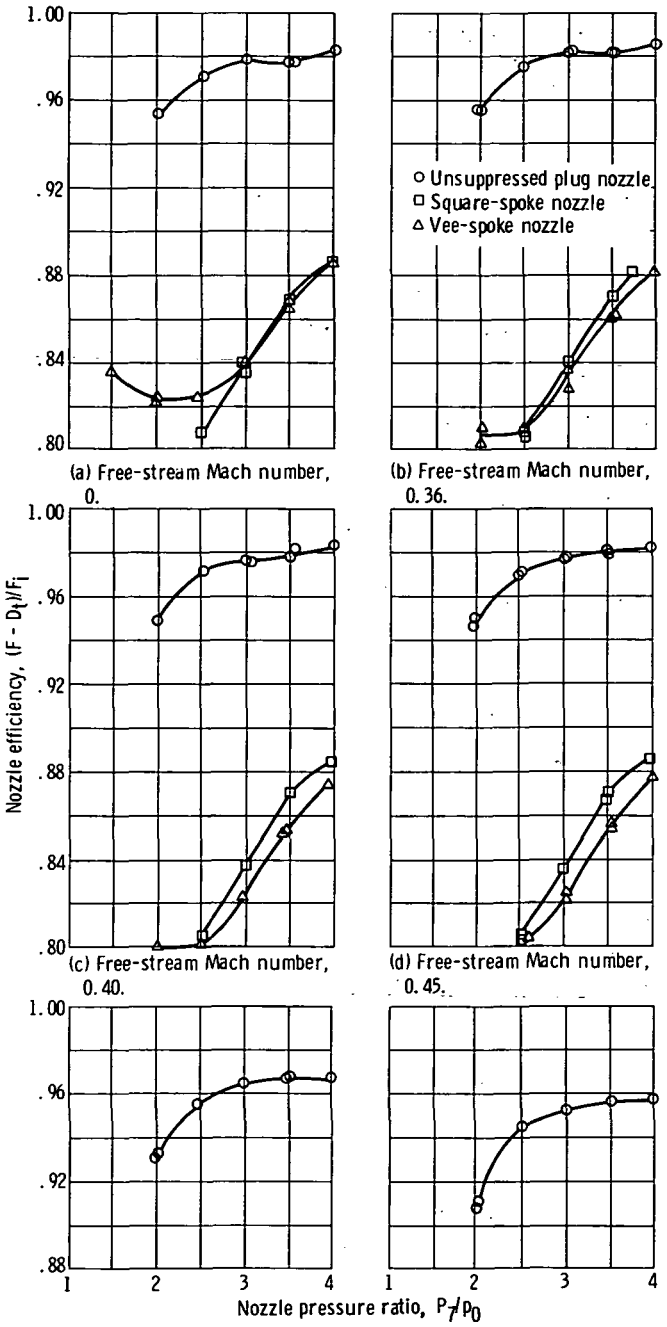

Figure 16. - Comparison of performance for unsuppressed plug nozzle and 40-spoke suppressor nozzles.

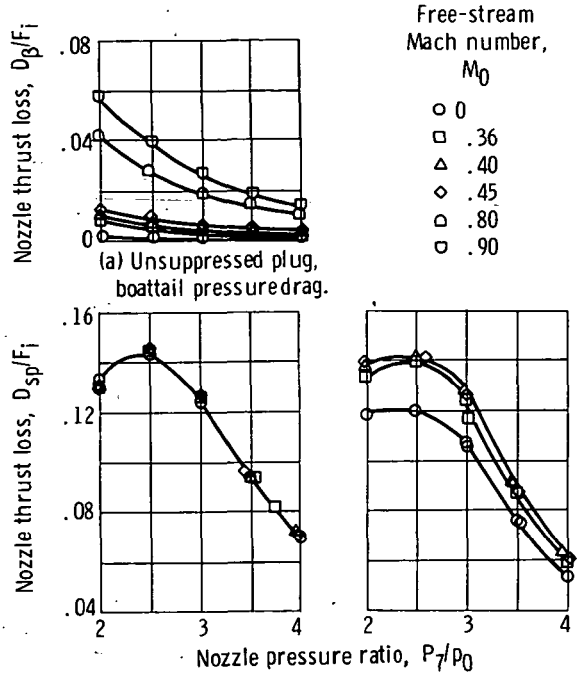

Figure 17. - Nozzle thrust loss from boattail or spoke-base pressure drag.

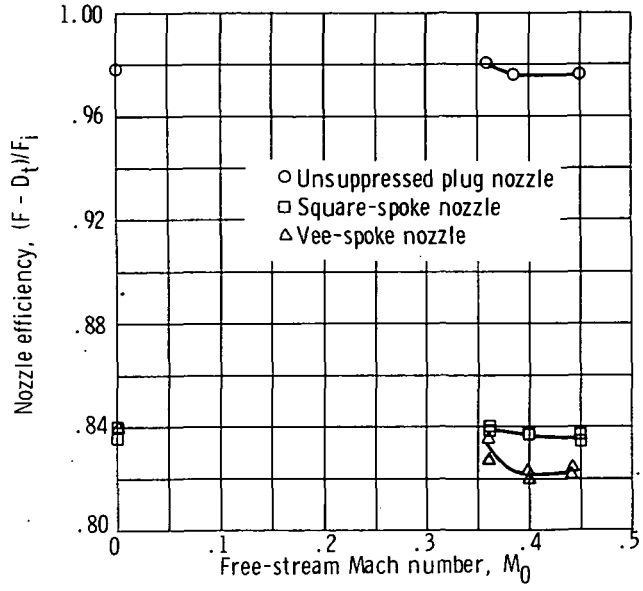

Figure 18. - External flow effects on nozzle performance. Nozzle pressure ratio, 3.0.

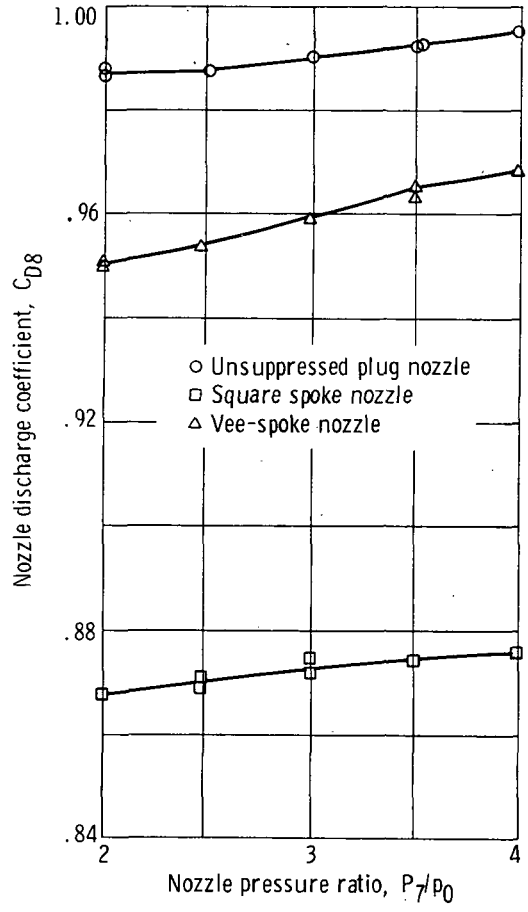

Figure 19. - Effect of nozzle pressure ratio on discharge coefficients.

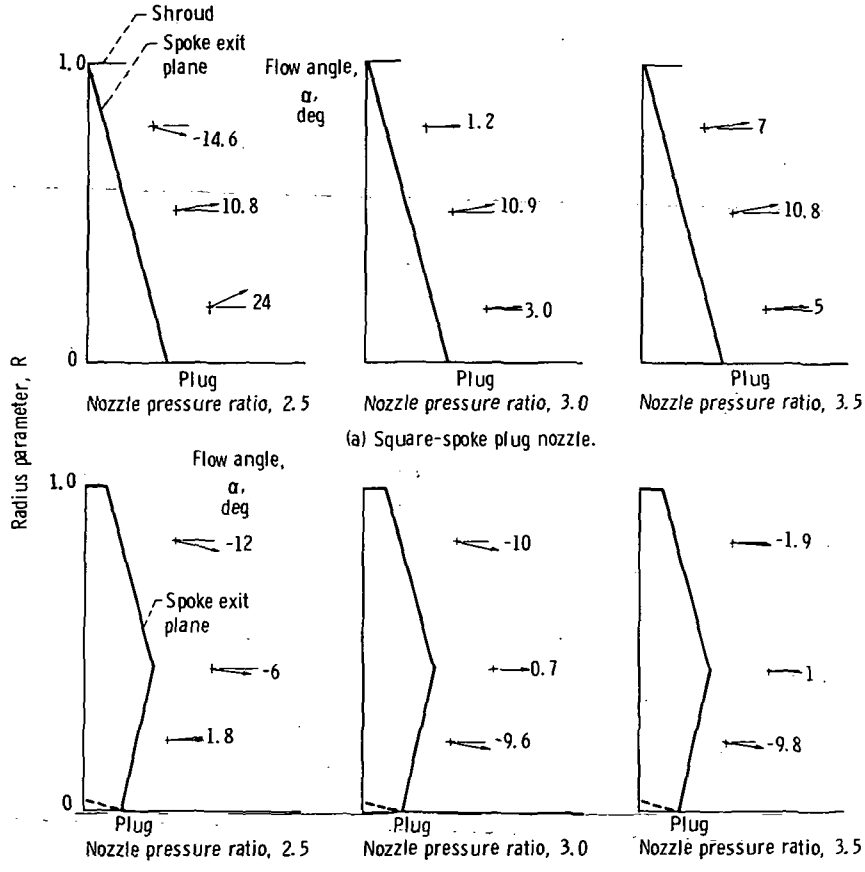

(a) Square-spoke plug nozzle.

(b) Vee-spoke plug nozzle.

Figure 20. - Nozzle-exit flow-angularity characteristics. $M_0 = 0$.

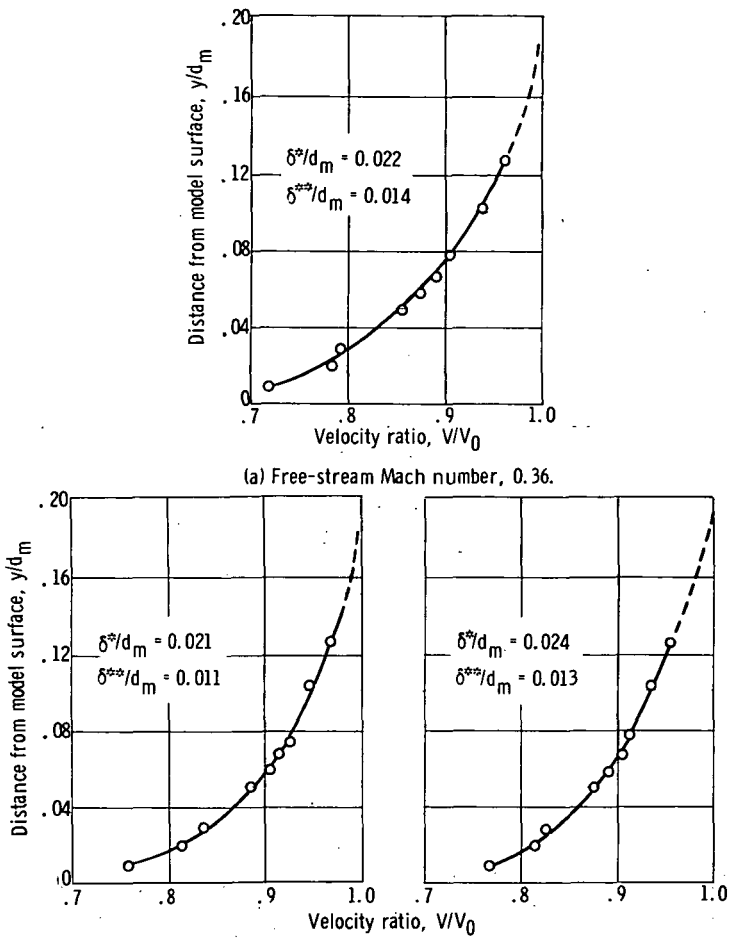

(a) Free-stream Mach number, 0.36.

(b) Free-stream Mach number, 0.80.

(c) Free-stream Mach number, 0.90.

Figure 21. - Boundary-layer velocity profiles at approximately nine nozzle diameters from nose of model.

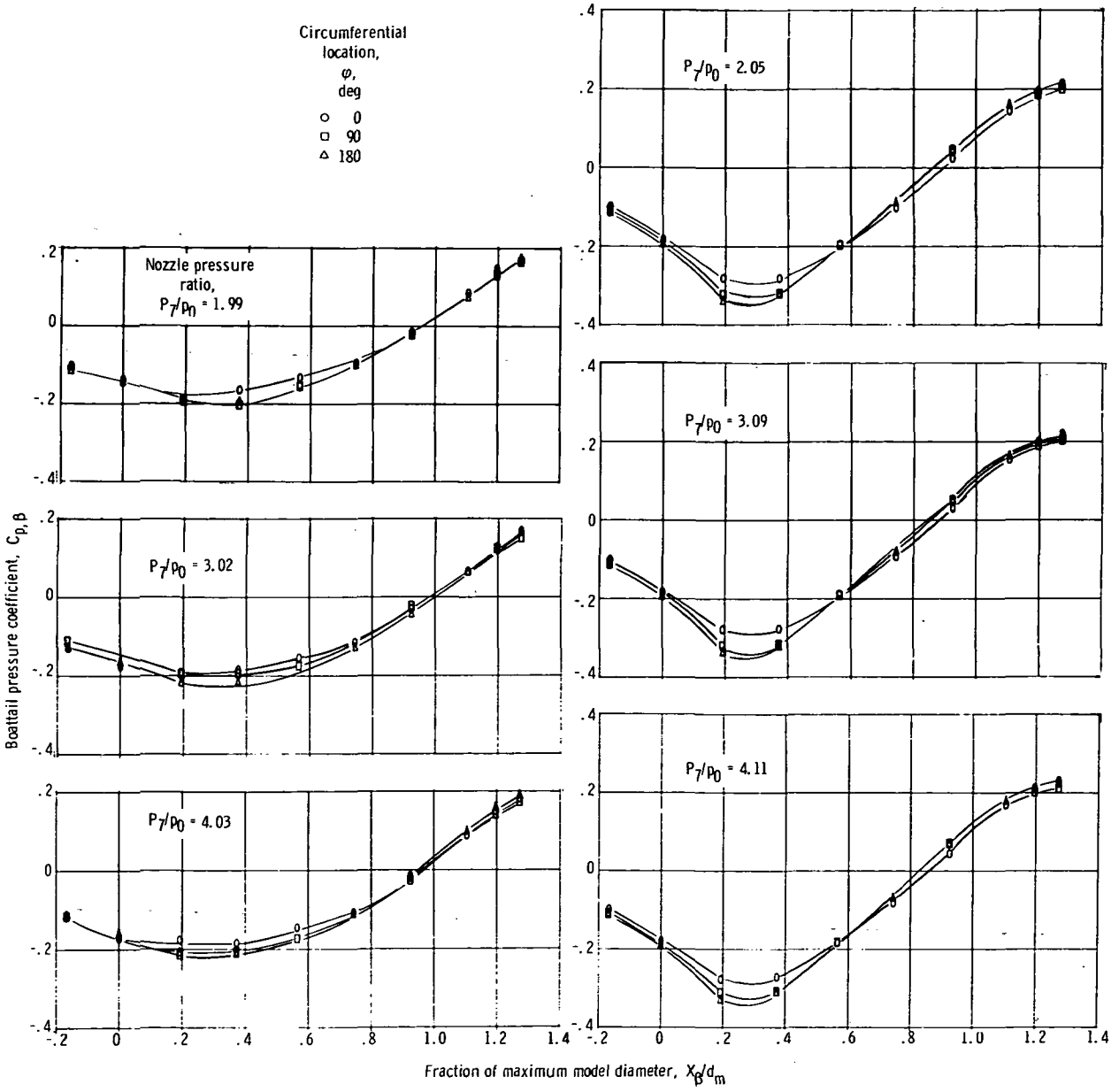

(a) Free-stream Mach number, 0.36.

(b) Free-stream Mach number, 0.90.

Figure 22. - Supersonic Tunnel Association (STA) nozzle boattail pressure distributions.

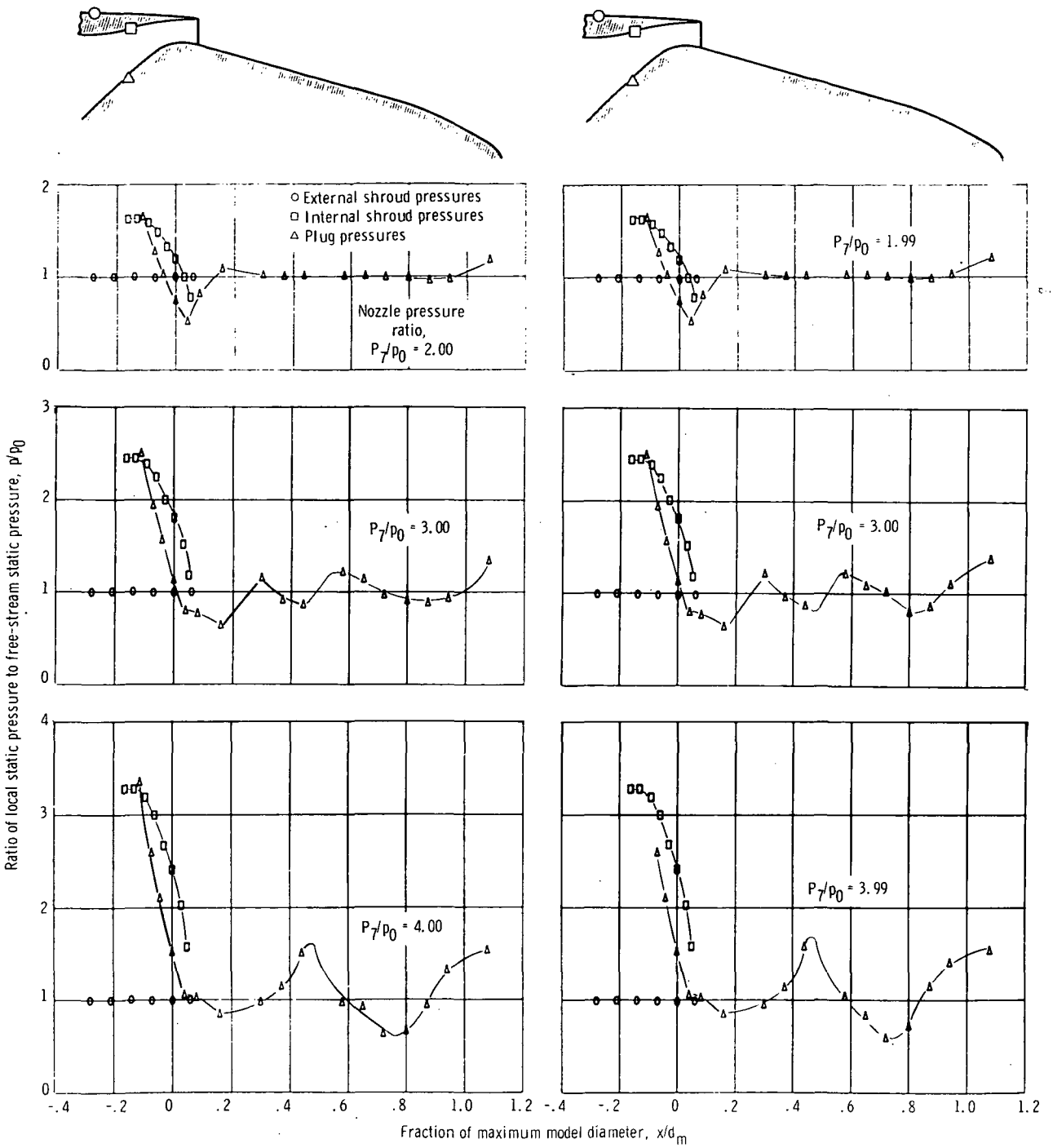

(a) Free-stream Mach number, 0.

(b) Free-stream Mach number, 0.36.

Figure 23. - Unsuppressed-plug nozzle surface pressure distributions.

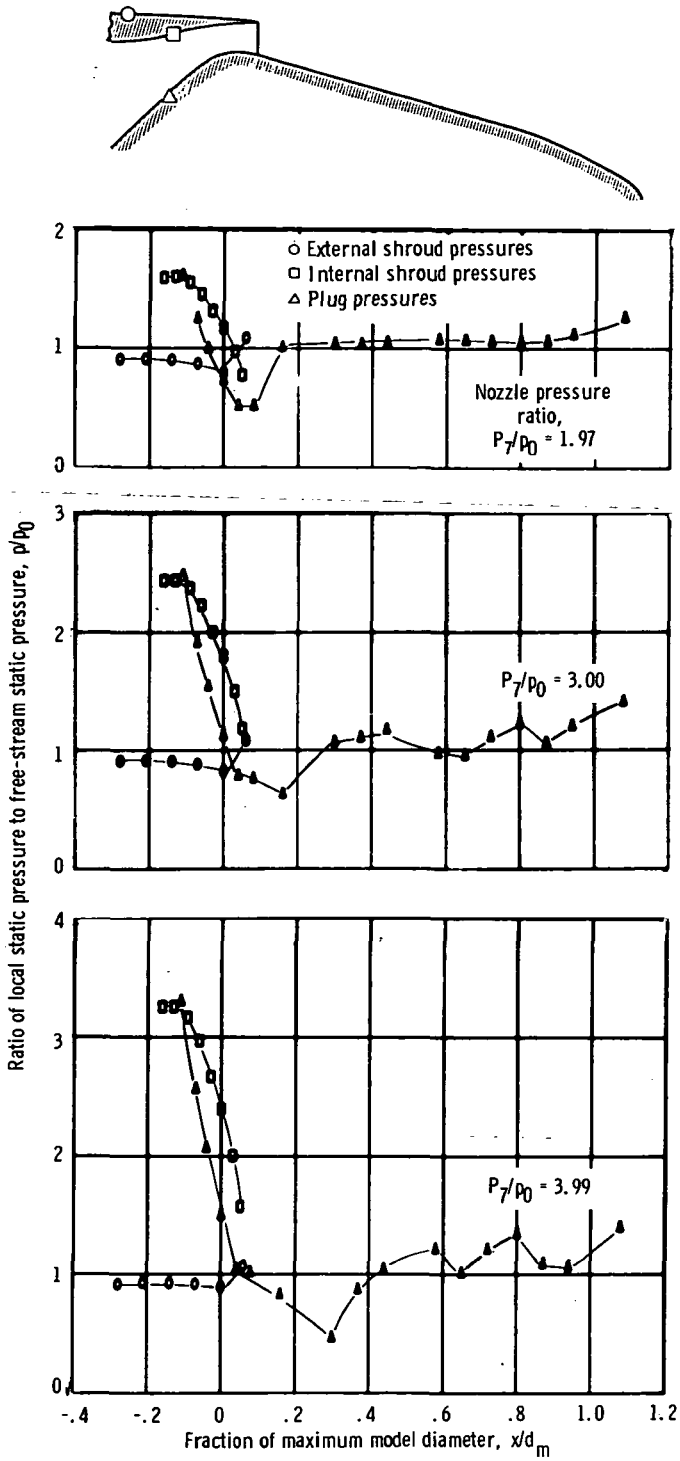

(c) Free-stream Mach number, 0.90.

Figure 23. - Concluded.

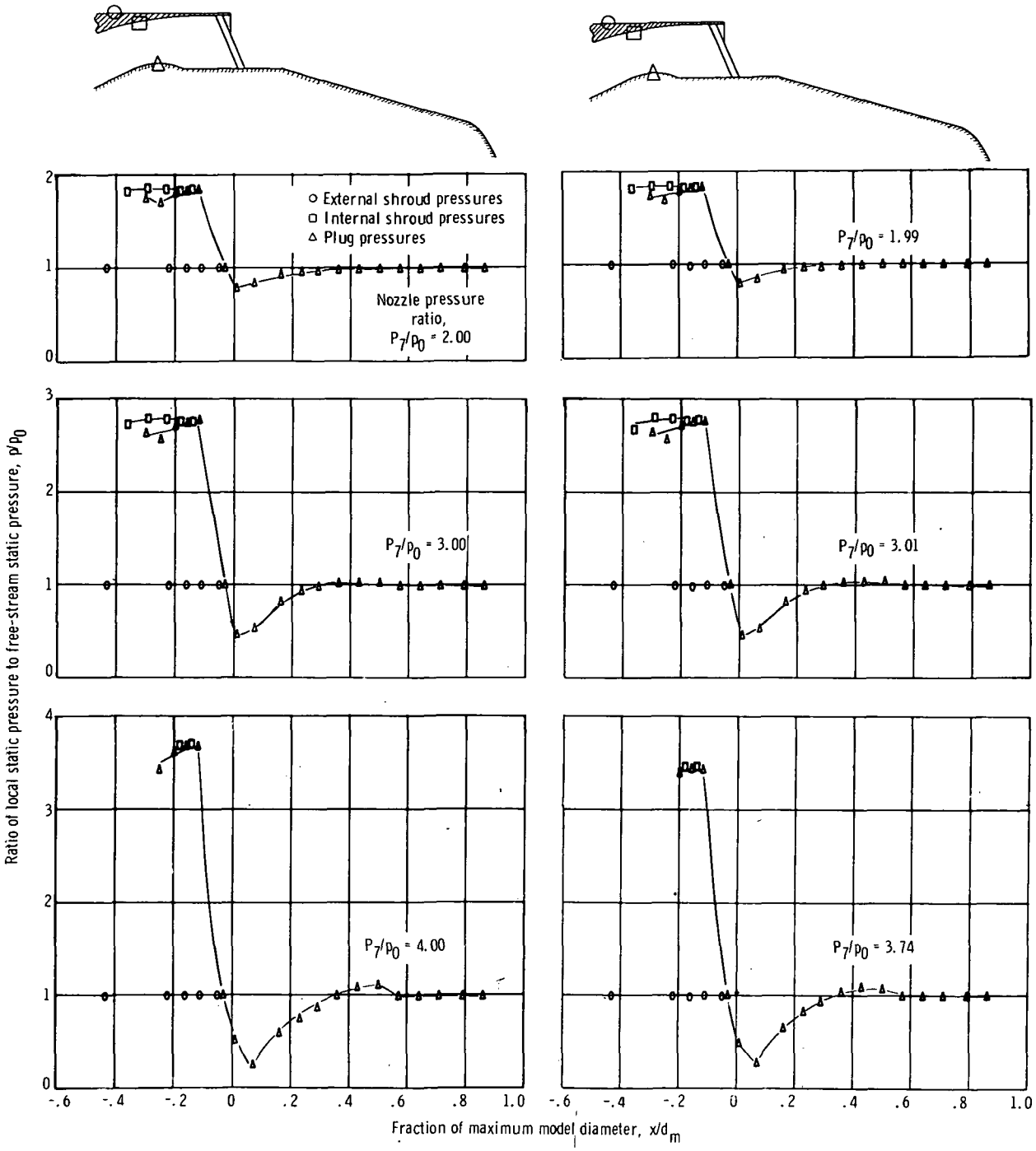

(a) Free-stream Mach number, 0.

(b) Free-stream Mach number, 0.36.

Figure 24. - Square-spoke plug nozzle surface pressure distributions.

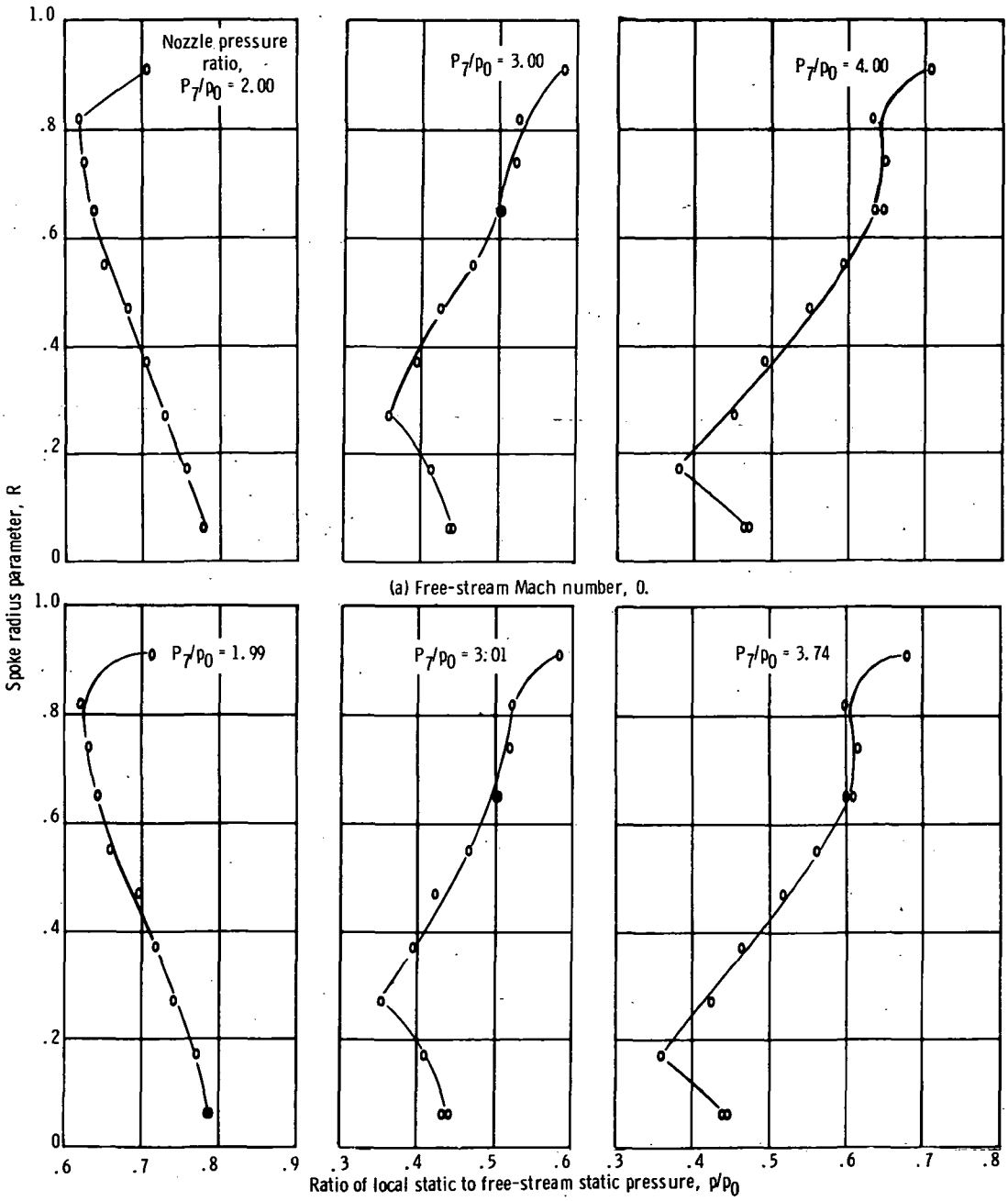

(a) Free-stream Mach number, 0.

(b) Free-stream Mach number, 0.36.

Figure 25. - Square-spoke plug nozzle, spoke-base pressure distributions.

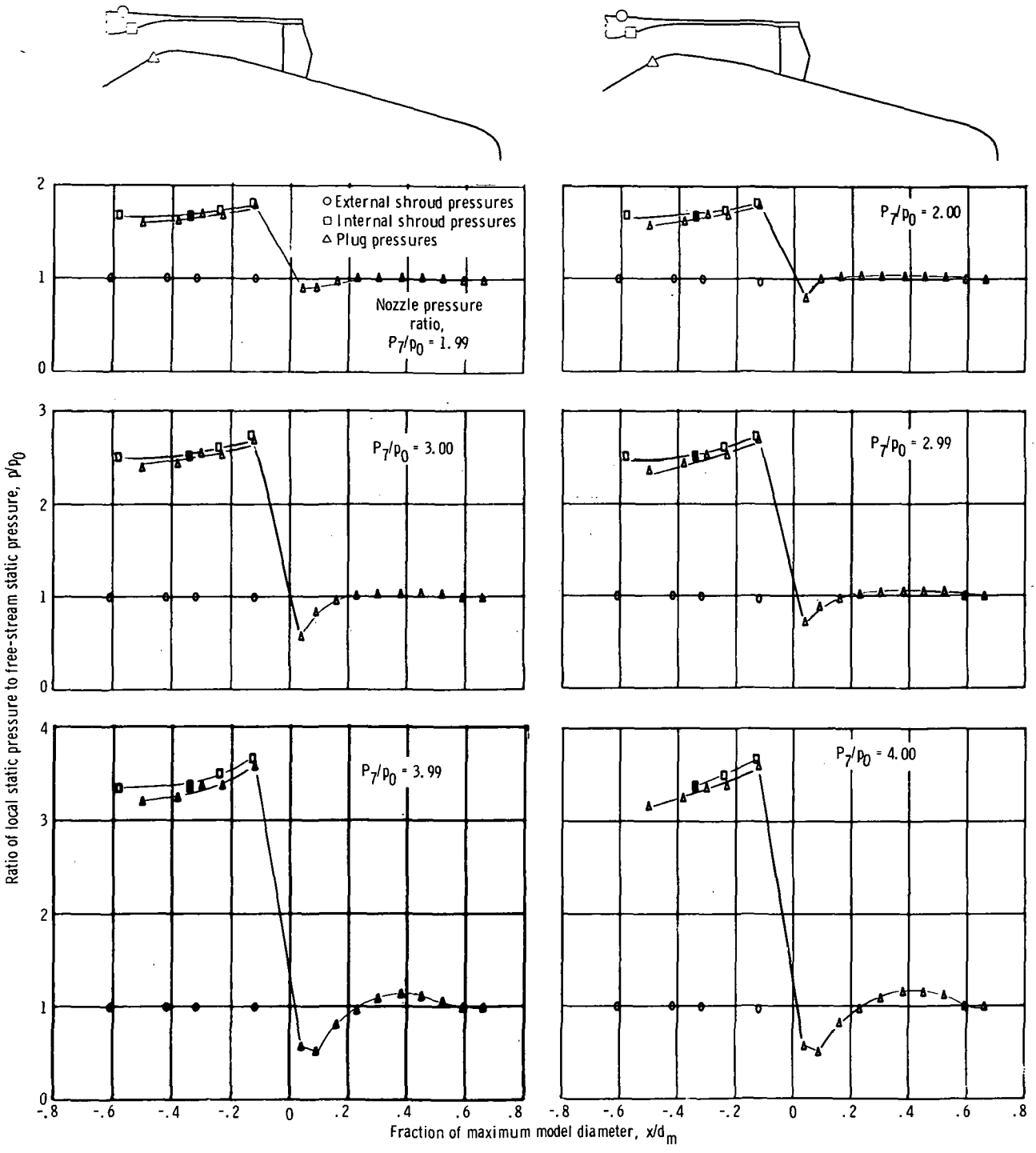

(a) Free-stream Mach number, 0.

(b) Free-stream Mach number, 0.36.

Figure 26. - Vee-spoke plug nozzle surface pressure distributions.

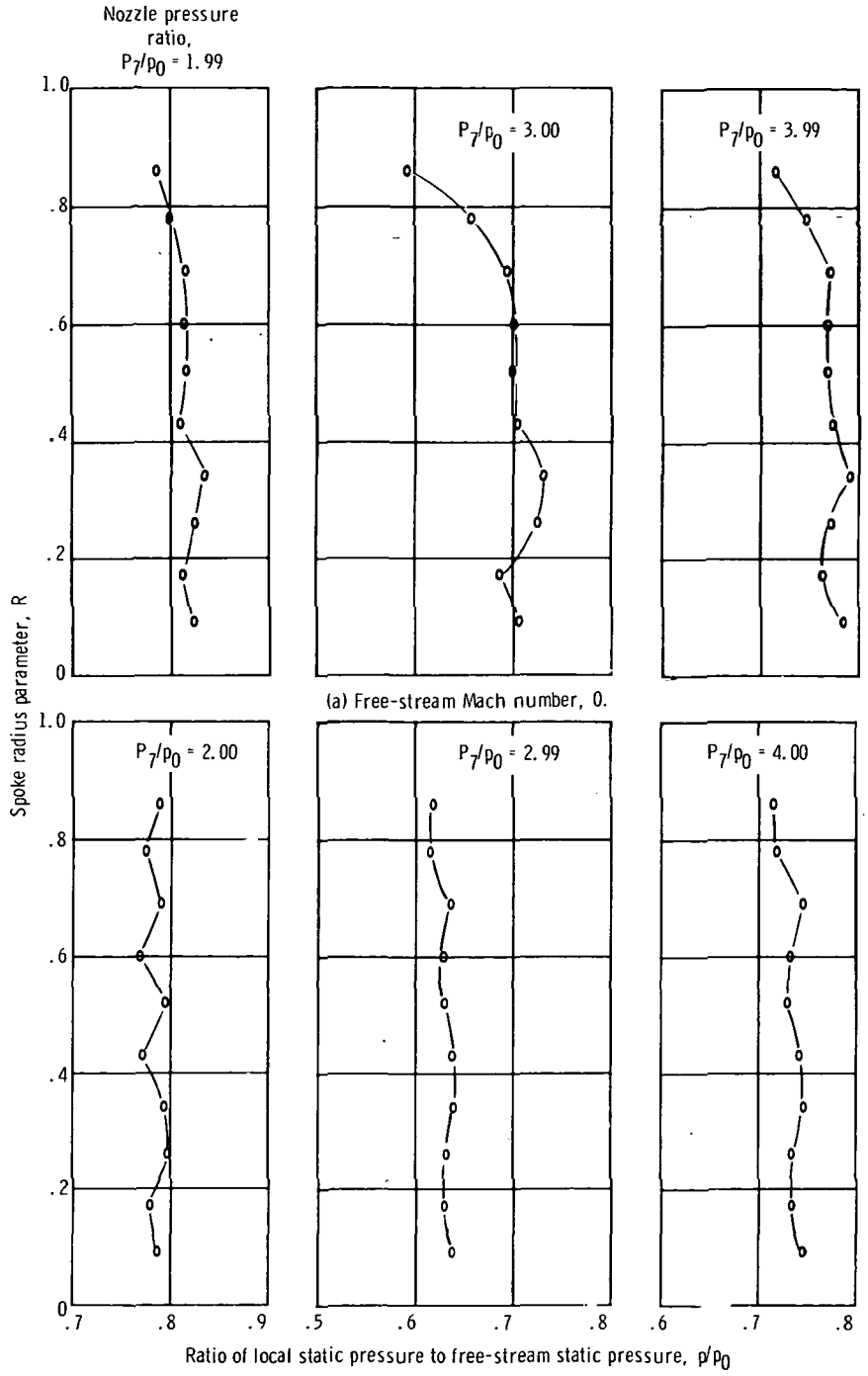

(a) Free-stream Mach number, 0.

(b) Free-stream Mach number, 0.36.

Figure 27. - Vee-spoke plug nozzle, spoke-base pressure distributions.

Page Intentionally Left Blank

Page Intentionally Left Blank

"The aeronautical and space activities of the United States shall be conducted so as to contribute . . . to the expansion of human knowledge of phenomena in the atmosphere and space. The Administration shall provide for the widest practicable and appropriate dissemination of information concerning its activities and the results thereof."

—NATIONAL AERONAUTICS AND SPACE ACT OF 1958

NASA SCIENTIFIC AND TECHNICAL PUBLICATIONS

TECHNICAL REPORTS: Scientific and technical information considered important, complete, and a lasting contribution to existing knowledge.

TECHNICAL NOTES: Information less broad in scope but nevertheless of importance as a contribution to existing knowledge.

TECHNICAL MEMORANDUMS: Information receiving limited distribution because of preliminary data, security classification, or other reasons. Also includes conference proceedings with either limited or unlimited distribution.

CONTRACTOR REPORTS: Scientific and technical information generated under a NASA contract or grant and considered an important contribution to existing knowledge.

TECHNICAL TRANSLATIONS: Information published in a foreign language considered to merit NASA distribution in English.

SPECIAL PUBLICATIONS: Information derived from or of value to NASA activities. Publications include final reports of major projects, monographs, data compilations, handbooks, sourcebooks, and special bibliographies.

TECHNOLOGY UTILIZATION PUBLICATIONS: Information on technology used by NASA that may be of particular interest in commercial and other non-aerospace applications. Publications include Tech Briefs, Technology Utilization Reports and Technology Surveys.

Details on the availability of these publications may be obtained from:

SCIENTIFIC AND TECHNICAL INFORMATION OFFICE

NATIONAL AERONAUTICS AND SPACE ADMINISTRATION

Washington, D.C. 20546